Suitability of ERA5-Land reanalysis dataset for hydrological modelling in the Alpine region

Daniele Dalla Torre [a], Nicola Di Marco [b], Andrea Menapace [a,*], Diego Avesani [c], Maurizio Righetti [a], Bruno Majone [c]

[a] *Faculty of Engineering - Free University of Bozen/Bolzano, Piazza Domenicani, 3, Bozen/Bolzano, 39100, Italy*
[b] *Dolomiti Energia Trading, Via Fersina, 23, Trento, 38123, Italy*
[c] *Department of Civil, Mechanical and Environmental Engineering - University of Trento, Via Mesiano, 77, Trento, 38123, Italy*

ARTICLE INFO

ABSTRACT

Study region: The region of interest is the South-Tyrol in the southeastern Alps, Italy. A comparison of meteorological forcing is performed with reference to this region while hydrological simulations are conducted in the Passirio river basin.

Study focus: The objective of this work is to evaluate the suitability of ERA5-Land reanalysis product as a reference dataset for hydrological modelling in topographically complex Alpine regions. ERA5-Land is compared with observational gridded dataset, obtained by means of the Kriging interpolation, available at two contrasting spatial resolutions a coarse grid size of 11×8 kilometres and a high-resolution grid size 1×1 kilometres. The hydrological coherence of the three datasets (ERA5-Land and the two observational datasets) with observed streamflow time series is then assessed with refer the Passirio/Passer river basin and to its nested and snow-dominated sub-catchment Plan/Pfelders.

New hydrological insights for the region: The study assesses ERA5-Land's suitability for hydrological simulations in the South-Tyrol region by comparing streamflow outcomes. At the annual scale, an overestimation of precipitation of about 40mm/month and a temperature underestimation of about 2.1 °C is reported. These discrepancies influence hydrological simulations, resulting in an overestimation of both streamflow and snow water equivalent. It is thus crucial to consider the limitations of ERA5-Land when using it as forcing for hydrological application in watersheds characterized by complex terrains, such as Alpine region.

1. Introduction

Hydrological models conceptualize complex natural processes related to the water cycle in a broad range of applications such as flood risk assessment (e.g. Apel et al., 2004; Barendrecht et al., 2017), hydropower production (e.g. Kouadio et al., 2022; Pandey et al., 2015; Avesani et al., 2021) and water management (e.g., Devia et al., 2015; Sood and Smakhtin, 2015). However, the reliability of hydrological simulations is strictly dependent on the correct spatial and temporal representation of the input meteorological forcing (Bisselink et al., 2016; Asong et al., 2020) aiming to properly reproduce the relevant hydrological processes over high-resolved domains and prolonged time windows (Ly et al., 2013; Arsenault and Brissette, 2014).

Nowadays, numerous gridded meteorological datasets are available, each one characterized by different spatio-temporal resolution and accuracy, with the latter being largely dependent on the type and amount of information used to obtain the product (e.g., Prein and Gobiet, 2017). Uncertainty stemming from the spatial distribution of the meteorological forcing propagates to hydrological modelling thus affecting the proper representation of hydrological variables (e.g., snow water equivalent and soil water content) (Maina et al., 2020; Shuai et al., 2022). Similarly, the temporal resolution of meteorological forcing exerts a strong control on the runoff generation and streamflow aggregation process. For example, streamflow modelling with high temporal resolution has been recognized as a key factor for flood forecasting (Wetterhall et al., 2011; Ficchì et al., 2016), in eco-hydrological studies (Woelber et al., 2018), and for the proper management of hydropower systems at sub-daily time scales (Xu and Liu, 2021; Avesani et al., 2022).

The control exerted by spatio-temporal resolution of gridded meteorological datasets on hydrological simulation soars in the Alpine context. Alpine Region is indeed characterized by heterogeneous landscapes and areas with highly variable topography, which may result in microclimatic variations (Tuo et al., 2016; Melsen et al., 2016). Local variations of both precipitation and temperature indeed control the snow accumulation and melting processes and in turn streamflow response, particularly in small headwater catchments (Khan et al., 2016; Ruelland, 2020). In this case, the hourly temporal resolution of meteorological forcing is thus mandatory to correctly simulate the diurnal snowmelt, which ensures regular streamflow supply to hydropower plants (Mahmud et al., 2019; Galletti et al., 2021).

So far, in situ measurements from meteorological stations have been the main provider of observational data for hydrological applications (Citterio et al., 2015). These are, however, not uniformly distributed in space, and data records are often inhomogeneous and limited in time (Hunziker et al., 2017). Meteorological stations are indeed usually deployed at low elevations to ease maintenance works and to guarantee optimal operational range (Hofstra et al., 2010). Furthermore, and despite the utmost importance of observational data for hydrological applications, a net decline in the number of meteorological stations was observed worldwide since the beginning of the 21st century due to installation and maintenance costs (Menne et al., 2018). Issues which are also present in the Alpine Region (Mallucci et al., 2019).

To compensate for the decreasing trend in the number of meteorological stations, interpolated datasets of precipitation and temperature are now routinely used. They allow to generate gridded information over continuous domains though the accuracy of the estimation depends strongly on network spatio-temporal coverage as well as on the type of interpolation algorithms adopted (Lespinas et al., 2015; Beck et al., 2020).

Alternatively, climate reanalyses are another type of product that has recently gained attention for obtaining gridded meteorological datasets (Qiaohong et al., 2017; Tetzner et al., 2019; Pelosi et al., 2020; Hafizi and Sorman, 2022). Those consist in retrospective numerical meteorological simulations of a past period combined with data assimilation procedures based on ground and satellite information. Differently from the interpolation method, the spatial and temporal structures of meteorological variables such as temperature and precipitation are reproduced on a physical and dynamical basis (Parker, 2016), which are consistent in space and time and are extended over long periods. Reanalyses could therefore be a useful product in areas where surface measurements are poor and unevenly distributed (Tarek et al., 2020; Essou et al., 2017; Muñoz Sabater et al., 2021). These products are routinely used as initial conditions for the generation of reforecasts products at the global scale (Hamill and Whitaker, 2006; Weerts et al., 2011), as reference datasets for the validation of short-term and seasonal forecast models (i.e., Crespi et al. (2021b)) and they are used as boundary conditions in climate model simulations (e.g., Xue et al. (2014)).

Several studies assessed the accuracy of reanalyses products in different regions by performing a direct comparison with observational datasets of precipitation or temperature. Illustrative examples are the works of Zandler et al. (2020), Hassler and Lauer (2021) and Tapiador et al. (2017) in the case of precipitation, Simmons et al. (2017) and Mistry et al. (2022) for temperature. All these studies concur that reanalysis products exhibit notable limitations, characterized not only by well-known biases due to modelling accuracy (mainly due to their typically low spatial resolution and to the poor representation of convection processes) but also by biases specific to the region of interest.

With reference to the Alpine Region, a limited number of studies investigated the accuracy and reliability of reanalysis products. Prömmel et al. (2010) and Scherrer (2020) demonstrated the superior performance of the ERA reanalysis temperature if compared with high-resolution regional climate simulations and regional reanalysis products (i.e. HARMONIE, MESCAN-SURFEX and COSMO-REA6). Regarding precipitation, Isotta et al. (2015) observed that regional reanalyses overestimates mean precipitation and the frequency of wet days in the Alpine region when compared to high-resolution station-based interpolation datasets. Most importantly, and to the best of the authors' knowledge, no studies have conducted an assessment of the suitability of these reanalysis products for hydrological modelling purposes in the Alpine region.

In order to fill the aforementioned gap, we have selected the ERA5-Land reanalysis dataset (Copernicus Climate Change Service, 2019) among other products (see National Center for Atmospheric Research, 2016, for an overview). On one hand, ERA5-Land represents the state-of-the-art global reanalysis dataset for land applications (Muñoz Sabater et al., 2021; Parker, 2016; Pelosi et al., 2020), and on the other is characterized by an higher spatial resolution compared to other products such as ERA5 (Hersbach et al., 2023) and the older ERA-Interim (Simmons et al., 2006), and thus making it more attractive for applications in areas characterized by complex topography.

This work has thus the following two objectives: (i) an assessment of the temperature and precipitation biases of the ERA5-Land product at the hourly resolution compared to a gridded observational dataset specifically developed for the study region; and (ii) an assessment of the suitability of ERA5-Land product for hydrological modelling in small Alpine catchments. To this aim, the river Adige basin with outlet in Bronzolo (Italy, Southern Alps) is chosen as a case study, which is referred to as South-Tyrol, hereafter. The region is characterized by an elevated number of meteorological stations, which allow for the elaboration of a reliable high

resolved in space and time gridded dataset by using kriging with external drift algorithm based on observational data (Goovaerts, 1997). The suitability of ERA5-Land for hydrological application is evaluated in the Passirio/Passer (Passirio hereafter) catchment. Passirio catchment exhibits indeed the typical features of alpine environments, including complex topography, high altitude, and a snow-dominated hydrological regime (Bellin et al., 2016; Majone et al., 2016) and thus it can be considered as a proxy of the typical hydrological response of the snow-dominated catchments located in the entire South-Tyrol (Nicòtina et al., 2008; Stergiadi et al., 2020).

The work objectives are pursued by developing an hourly gridded observational dataset of precipitation and temperature with a spatial resolution of 1 kilometre. Afterwards, the observational dataset is upscaled to the spatial resolution of ERA5-Land for a fair comparison with the reanalysis dataset as well as to evaluate the sensitivity of meteorological-forcing resolution on hydrological simulations in a snow-dominated alpine catchment.

The suitability of the various considered datasets for hydrological modelling is evaluated by adopting the recently introduced Hydrological Coherence Test (HyCoT) (Laiti et al., 2018) method, which provides a framework for excluding meteorological datasets not coherent with streamflow observations as a function of the modelling goal at hand. In particular, we analysed the hydrological performances of three datasets: ERA5-Land, the gridded observational data produced by kriging evaluated at the original resolution of 1 km, and at the same coarse scale of ERA5-Land. It is worth mentioning that the hourly dataset at 1 km spatial resolution obtained by kriging is novel for the analysed region, and it also represents a valuable benchmark for future hydrological applications and analysis in this region.

The article is organized as follows. Section 2 describes the case study, while Section 3 introduces both the different types of data used and the methods, including the kriging algorithm, the hydrological model, the hydrological coherence procedure and the experimental design of the simulations. Section 4 presents the results of the meteorological comparison and of the hydrological simulations. Section 5 presents an extensive discussion about the performance of ERA5-Land in hydrological modelling, and finally in Section 6 conclusive remarks are drawn.

2. Case study

This work is carried out in the Autonomous Province of Bolzano/Bozen (South-Tyrol hereafter), an Italian province located in the southeastern Alps, Italy (see Fig. 1). A complex mountainous topography characterizes the territory of the Province with deep valleys and high mountain crests. Watercourses of the main valleys converge into the main river of the region, the Adige, which rises at Resia/Reschen pass and ends its course after 409 km into the Adriatic sea at Rosolina a Mare (Chiogna et al., 2016). Adige river basin closed at Bronzolo/Branzoll (Bronzolo hereafter) gauging station has a contributing area of 6926 km^2, accounting for 59% of the total contributing river basin area (Autorità di Bacino Nazionale del Fiume Adige, 2008). The climate of South-Tyrol is continental with warm and wet summers and cold and dry winters as typical in the Alpine Region (Lutz et al., 2016; Diamantini et al., 2018). Average annual precipitation during the period 2010–2019 is 941 mm, while average monthly temperatures range from the minimum of −4.02 °C in winter to the mean maximum of 15.03 °C in summer.

Hydrological analyses are carried out in the Passirio catchment, one of the main tributaries of the Adige river along its course in the South-Tyrol (Stergiadi et al., 2020), with reference to the Merano/Meran (Merano hereafter) and Plan/Pfelders (Plan hereafter) gauging stations, respectively (see Fig. 1). The catchment closed at Merano has a drainage area of 414 km^2 with elevation ranging from 365 m a.m.s.l. to 3380 m a.m.s.l.. The nested sub-catchment closed at the Plan gauging station has an area of 49 km^2 and higher elevation, which ranges between 1440 m a.m.s.l. and 3380 m a.m.s.l.. The mean annual precipitation in the Passirio catchment during the period of interest is approximately 1150 mm, and thus in line with the annual average precipitation of the entire South Tyrol (Chiogna et al., 2016; Mallucci et al., 2019). The precipitation distribution follows the typical pattern observed across the Adige river basin (Laiti et al., 2018), with the majority of precipitation occurring in the summer and autumn seasons. The Passirio has a typical snow-dominated hydrological regime with high flows during the melting season and in the autumn triggered by cyclonic storms (Norbiato et al., 2009; Di Marco et al., 2021; Larsen et al., 2021). The Passirio catchment is known for its hydrological regime that primarily relies on quick subsurface flow and surface runoff generation (Stergiadi et al., 2020; Avesani et al., 2022).

3. Data and methods

3.1. Observational data

Hourly temperature and precipitation data were provided by the Meteorological Office of the Autonomous Province of Bolzano/Bozen (Italy) (https://meteorological.provinz.bz.it/meteorological-stations-valley.asp). Specifically, temperature and precipitation time series were available at 177 and 129 stations, respectively (see Fig. 1), during the time window 2010–2019.

The distribution of the stations covers the entire area of interest with a mean horizontal distance among them of 2.9 km. The 86 % of the ground stations are located under 2300 m a.m.s.l. leaving the highest elevations less monitored as shown in Fig. 2. It can also be noted a preponderance of temperature stations compared to precipitation stations for high altitudes, whereas the highest number of meteorological stations (22 out of 177 for temperature and 27 out of 129 for precipitation) is located at altitudes between 750 m a.m.s.l. and 1000 m a.m.s.l.. Changes in the number of meteorological stations with the elevation and their effect on the hydrological simulations will be further discussed in Section 5.

Streamflow records during the period 2010–2019 were provided by the Hydrological Office of the Autonomous Province of Bolzano/Bozen (Italy) (https://weather.provinz.bz.it/gauging-stations.asp) at the gauging stations of Merano and Plan in the Passirio
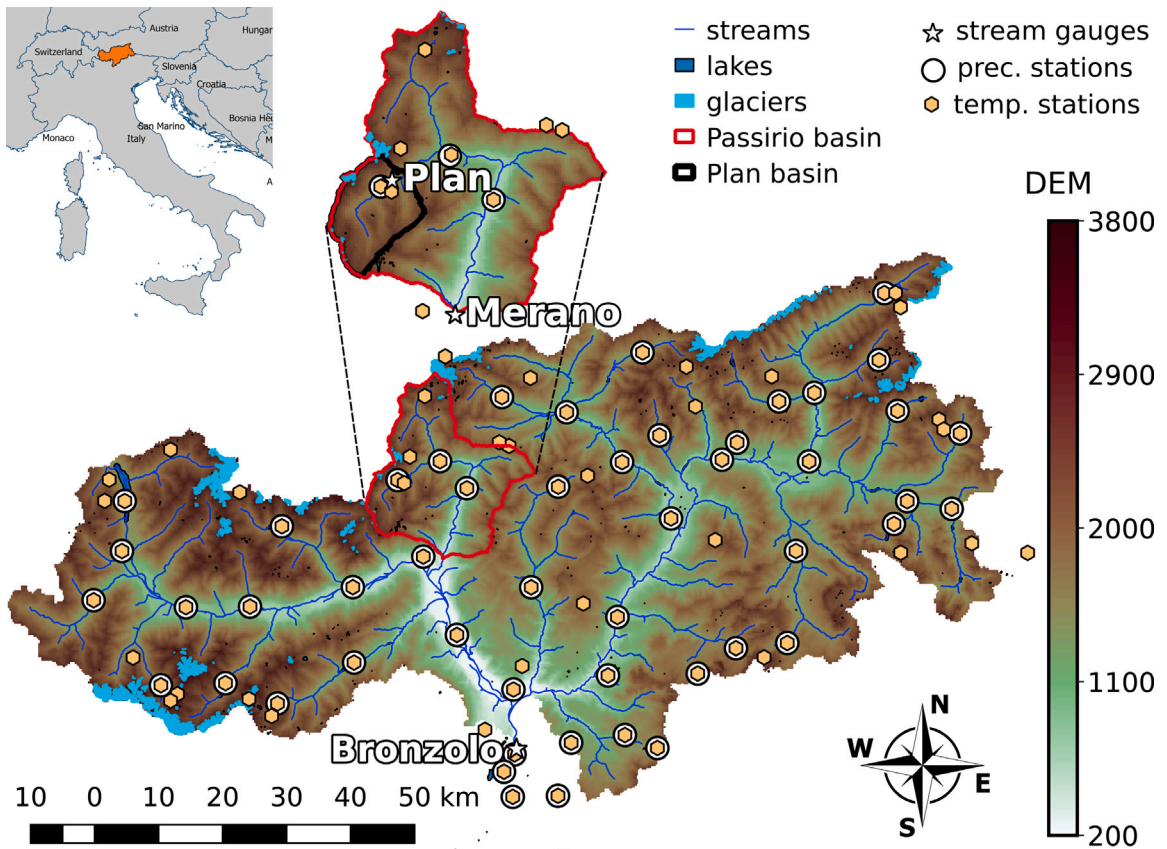
Fig. 1. Map of the Adige river catchment with the outlet being located in Bronzolo (South-Tyrol). The maps also shows the Digital Elevation Model (DEM) of the region, the river network, and the meteorological and stream gauging stations. The inset shows the Passirio catchment closed at Merano and the nested sub-catchment of Plan.
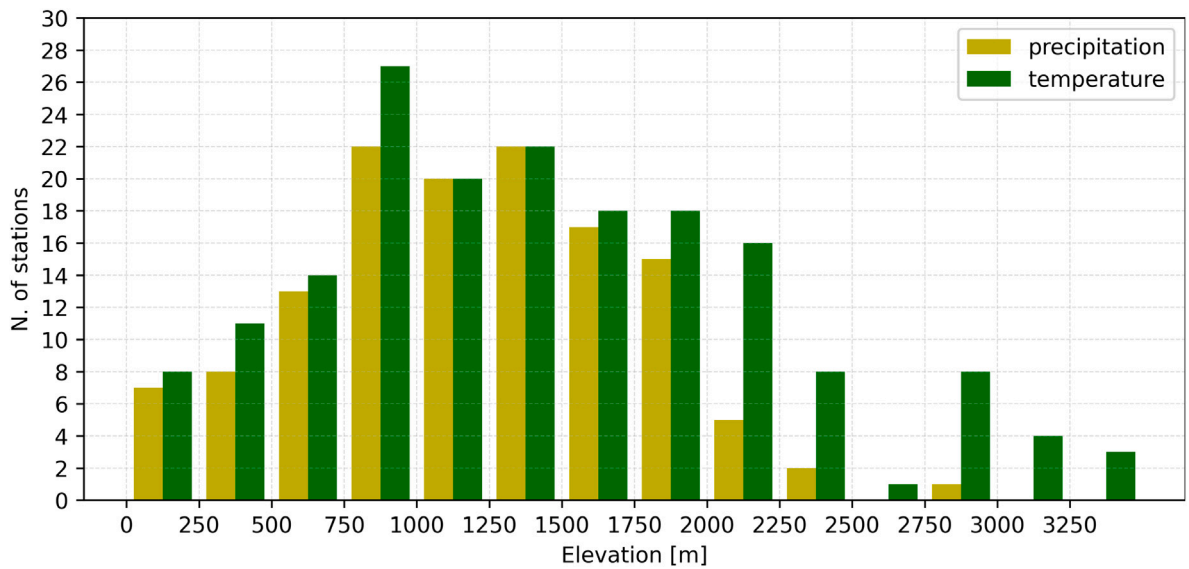

Fig. 2. Distribution of ground stations per elevation band for temperature and precipitation in the South-Tyrol area. Each bin represents an elevation band range of 250 m, spanning from 0 m a.m.s.l. to 3500 m a.m.s.l..

Table 1

Parameters of the exponential covariance model for hourly precipitation and temperature data in the study region.

Variables	Precipitation	Temperature
σ_n^2	$0.742 \, \text{mm}^2$	$6.492 \, °\text{C}^2$
σ^2	$2.882 \, \text{mm}^2$	$21.117 \, °\text{C}^2$
a	$15\,699 \, \text{m}$	$104\,126 \, \text{m}$

catchment. These are official measurements and are characterized by a limited number of missing data. Records at Merano are used to calibrate the hydrological model and to evaluate the suitability of the different datasets adopted in this work. Data at Plan are used to provide a spatial validation of the proposed framework in a nested sub-catchment, where the streamflow data are available but not used in the parameter estimation phase (Di Marco et al., 2021). The mean metered streamflow at Merano gauging station is $12.04 \, \text{m}^3/\text{s}$, with a minimum of $0.64 \, \text{m}^3/\text{s}$ registered in March 2018 and a maximum of $119 \, \text{m}^3/\text{s}$ in June 2014. The mean metered streamflow at Plan sub-catchment closure is $2.25 \, \text{m}^3/\text{s}$, with a minimum value of $0.26 \, \text{m}^3/\text{s}$ in March 2016 and a maximum of $19.85 \, \text{m}^3/\text{s}$ in June 2016.

3.2. ERA5-Land data

Reanalyses data used in this work is the ERA5-Land product (Muñoz Sabater et al., 2021), which is the last generation reanalysis from ECMWF recently released on Copernicus portal (Copernicus Climate Change Service, 2019). Data were retrieved for the period 2010–2019. It is generally considered a reference climate product for a wide range of applications including, for example, assessment of crop-reference evapotranspiration (Pelosi et al., 2020), estimation of soil moisture (Madhavi et al., 2022) and hydrological modelling at the global scale (Parker, 2016; Muñoz Sabater et al., 2021). The performances of the companion product ERA5 in reproducing precipitation extremes over complex orography terrains have recently validated by Mastrantonas et al. (2022). ERA5-Land provides, among many variables, hourly time series of temperature and precipitation with a $0.1° \times 0.1°$ grid spacing horizontal resolution. This resolution is achieved through numerical integration of the ECMWF land surface model driven by the downscaled meteorological forcing from the ERA5 climate reanalysis, including an elevation correction for the thermodynamic near-surface state, which allows for a better reproduction of the climate condition at the local scale (Xie et al., 2022). In this context, it is worth mentioning the existence of the dataset VHR-REA_IT (Raffa et al., 2021), which has been recently developed at the resolution of about $2.2 \, \text{km}$ as a dynamical downscaling of ERA5 by means of a convection-permitting climate model. The dataset is able to reproduce rainfall extremes better than ERA5 (Reder et al., 2022), though its performances are yet to be demonstrated in hydrological applications. For this latter reason and also considering its recent release, we still opted to use ERA5-Land for the proposed analysis.

In the proposed work, the ERA5-Land dataset is transformed through a rototranslation of the cells composing the grid, from the original $WGS84$ reference coordinate system to $ETRS8$ reference system. The original horizontal resolution ($0.1°$), equivalent to around $9 \, \text{km}$ regular grid, thus results in an almost rectangular grid of $11 \times 8 \, \text{km}$. This dataset is referred to as REA11×8 hereafter.

3.3. Interpolation of observed meteorological data

To obtain the spatial distribution of the observational data, the hourly precipitation and temperature data available at the meteorological stations were interpolated over a regular $1 \, \text{km}$ grid using a kriging algorithm (KR). Among the different kriging schemes, the interpolation was performed using the kriging with the terrain elevation as external drift for both temperature and precipitation (Goovaerts, 1997). Specifically, the interpolation was performed by using gaussian, exponential and spherical covariance functions combined with a nugget model and considering measurements available at the closest 8, 16, and 32 meteorological stations. A leave-one-out cross-validation procedure was then applied to all the aforementioned configurations to identify the geostatistical model configuration leading to the smallest error over the period 2010–2019. The procedure allowed to identify kriging with 16 neighbouring stations and the exponential covariance model with nugget as the most accurate interpolation scheme for both precipitation and temperature. The Eq. (1) reports the covariance function herein adopted:

$$C(r) = \sigma_n^2 \delta(r) + \sigma^2 exp\left[-\frac{3r}{a}\right];$$
(1)

where r is the two-point lag distance, $\delta(r)$ characterizes the nugget effect and it reads as follows: $\delta(r) = 1$ if $r = 0$ and $\delta(r) = 0$ if $r \neq 0$, σ_n^2 and σ^2 are the variances at small (i.e., the nugget) and large scales, respectively, while a is a scaling parameter. For the sake of completeness, Table 1 reports the values of the parameters of the geostatistical models, providing the lowest cross-validation errors for the temperature and precipitation. The obtained gridded hourly dataset of precipitation and temperature is hereafter referred to as KR1×1.

The outcomes of the cross-validation procedure are reported in Section 4.1. Specifically, two widely used metrics were adopted, namely the Mean Absolute Error (MAE) and the Mean Error (ME) defined as follows (Murphy, 2012):

$$MAE = \frac{1}{n} \sum_{i=1}^{n} |p_i - a_i|$$
(2)

Table 2

List of ICHYMOD model parameters for snow and rainfall-runoff modules (respectively TOPMELT and PDM models, respectively).

Name	Unit	Range	Description	Sub-model
PCF	–	1–1.2	Precipitation Correction Factor	TOPMELT
CMF	$\dfrac{mm\,m^2}{MJ\,h\,°C}$	0.001–0.1	Combined Melt Factor	TOPMELT
G	$\dfrac{mm}{km}$	0–0.5	Precipitation gradient with altitudes	TOPMELT
alb_s	–	0.70–0.95	Fresh snow albedo	TOPMELT
T_c	°C	0–2.5	Threshold temperature for rain/snow classification	TOPMELT
RMF	$\dfrac{1}{h\,°C}$	0.01–0.90	Rain Melt Factor	TOPMELT
C_{max}	mm	100–550	Maximum storage capacity	PDM
b	–	0.025–0.75	Storage capacity probability density function exponent	PDM
K_g	$\dfrac{hh\,mm^{b_s}}{mm}$	18k–60k	Groundwater recharge time constant	PDM
b_g	–	1.3–2.3	Exponent of groundwater recharge function	PDM

$$ME = \frac{1}{n}\sum_{i=1}^{n}(p_i - a_i) \tag{3}$$

where p_i is the reconstructed value, a_i is the observed value at the ith time step and n is the length of the series.

3.4. ICHYMOD hydrological model

The semi-distributed hydrological model ICHYMOD (Integrated catchment-scale hydrological model Norbiato et al., 2008, 2009) is used to simulate hydrological processes at the hourly time scale in the Passirio catchment. ICHYMOD has already proven to be a reliable tool over the region of interest for the accurate prediction of both streamflow and snow variables (Zaramella et al., 2019; Di Marco et al., 2020, 2021; Avesani et al., 2022). This model adopts a semi-distributed approach where the catchment is divided into several sub-catchments in which the hydrological properties are assumed uniform. Different modules are embedded in the ICHYMOD framework to simulate the overall hydrological cycle at an hourly time step. Potential evapotranspiration is estimated with the Hargreaves formula (Hargreaves and Samani, 1985), while snowpack dynamics are computed by means of the TOPMELT model, recently developed by Zaramella et al. (2019). The PDM approach (Moore, 2007) is used for modelling rainfall-runoff transformation taking water of snow–ice melting dynamics (TOPMELT model) and evapotranspiration (Hargreaves module) to recharge groundwater. The Muskingam–Cunge scheme is adopted for streamflow routing along the river network (Cunge, 2010). More details on TOPMELT are reported below to allow a clearer discussion of the results.

TOPMELT integrates both snow and ice melting dynamics into the ICHYMOD by means of an enhanced temperature-index approach. It is important to mention that TOPMELT divides the sub-catchment into elevation bands, whose pixels are then aggregated into uniformly distributed radiation classes. This allows both air temperature and precipitation variability with elevation to be taken into account. Specifically, the snowmelt F for the ith elevation band and the jth radiation class at time t is calculated as follows:

$$F_{i,j}(t) = \begin{cases} CMF \cdot RI_{i,j}(t)\left(1 - alb_s(t)\right) \cdot max\left[0; T_i(t) - T_c\right], & \text{if } t \in \text{daytime} \\ NMF \cdot max[0, (T_i(h) - T_c)], & \text{if } t \in n \text{ nighttime} \end{cases} \tag{4}$$

where $T_i(t)$ is the air temperature of the ith elevation band; $RI_{i,j}(t)$ is the cell radiation index; CMF is the Combined Melt Factor; alb_s is the snow albedo; T_c is a threshold base temperature; and NMF is the night melt factor. Furthermore, the snow model accounts for both rain-on–snow, ice melting, and water refreezing (see Zaramella et al. (2019) for further details). Estimated precipitation and air temperature time series at each elevation band are then used to calculate snow accumulation. Specifically, precipitation is divided into rainfall and snowfall depending on the threshold temperature, T_c. Then, either a precipitation correction factor (PCF) or a snow correction factor (SCF) are applied to account for spatial representativeness and potential deficiencies during periods of snow. The precipitation value $P_i(t)$ at the ith elevation band is thus computed as follows:

$$P_i(h) = P_{avg}(t) \cdot \left(1 + \left(z - z_{avg}\right) \cdot G\right) \tag{5}$$

where P_{avg} is the mean areal total precipitation over a specific sub-catchment, z is the elevation band altitude and z_{avg} is the sub-catchment mean elevation. The term G is instead the precipitation lapse rate, which is assumed constant and computed at the regional scale from the available precipitation data.

Temperature T_i over the ith band is computed by using an hourly time-varying vertical temperature lapse rate, $LR(t)$, which is unique for the entire basin and obtained from available temperature data. Indeed, a linear regression process is performed at each hourly time step using recorded temperature and the corresponding station altitude.

For a more comprehensive presentation of the other modules of the model, readers are referred to the works of Moore (2007) and Norbiato et al. (2008). Table 2 reports the main parameters of ICHYMOD, including their units, ranges of variation, and sub-model use. As described in Section 3.6, 9 of these parameters are estimated through model calibration, G is instead evaluated a priori. PCF and T_c are reported in this table for description consistency but are not calibrated because this paper's goal is to compare the different meteorological datasets without introducing a correction factor in the inversion procedure.

Table 3

Summary of datasets used in the present work, with P and T representing precipitation and temperature variables, respectively. The table provides an overview of the representative acronyms, variables comprising each dataset, the data source, and the temporal/spatial resolutions.

	KR1×1	KR11×8	REA11×8
Variables	P, T	P, T	P, T
Type of data	Interpolated station data	Aggregated KR1×1	ERA5-Land model
Spatial resolution	1 × 1 km	11 × 8 km	11 × 8 km
Temporal resolution	Hourly	Hourly	Hourly

3.5. Hydrological Coherence Test (HyCoT)

The evaluation of the meteorological datasets utilized in this study for hydrological modelling is conducted using the Hydrological Coherence Test (HyCoT) (Laiti et al., 2018). This method employs a goal-oriented framework to discern meteorological forcing datasets that do not align with hydrological observations. Essentially, the hydrological model outcomes serve as a tool to assess the "hydrological coherence" between precipitation and observational variables. A model calibration is performed for each meteorological forcing dataset available, enabling the comparison of the hydrological model outcomes according to a chosen metric, thus evaluating the feasibility of the meteorological forcing in allowing the reproduction of the observed variables.

In this study, the Nash–Sutcliffe Efficiency (NSE hereafter) index (Nash and Sutcliffe, 1970) is adopted as the efficiency metric, with streamflow serving as the observational variable. It is important to note that the model calibration, performed individually for each meteorological forcing dataset, utilizes the Generalized Likelihood Uncertainty Estimation (GLUE) methodology (Beven and Binley, 1992). This involves employing a Monte Carlo sampling approach to generate numerous parameter sets randomly from the parameter space, each representing a plausible combination of parameter values. Subsequently, the hydrological model is executed for each parameter set, producing model outcomes (in this case, streamflows) for each simulation. These model results are then compared to the observed streamflows using the adopted efficiency metric to identify the parameter set that ensures the best performance.

3.6. Experimental design

In order to evaluate the accuracy of REA11×8 dataset in the entire South-Tyrol region, the observational dataset KR1×1 is resampled by areal averaging to the same grid of REA11×8. This upscaled version of the observational dataset is hereafter termed as KR11×8. Overall, we thus considered three meteorological input forcing datasets as summarized in Table 3. An assessment of the bias is then performed on the period 2010–2019 by considering cell-to-cell difference between REA11×8 and KR11×8, while the t-test (Lehmann and Romano, 1986) is applied to assess the correlation between biases and elevation with a level of significance of 0.05.

Evaluation of the hydrological coherence of the three datasets (i.e. REA11×8, KR11×8 and KR1×1) was performed on the Passirio catchment by considering an hourly time step. According to the ICHYMOD framework, the catchment is partitioned into 23 sub-catchments with an average area of $20 \, km^2$. As shown in Fig. 3, three of these sub-catchments constitute the nested sub-catchment of Plan, adopted for the spatial validation (see Section 4.3).

It is worth noticing that for each dataset (i.e. REA11×8, KR11×8 and KR1×1) the corresponding precipitation lapse rate G was computed considering the entire South-Tyrol and it is assumed constant in space and time. The decision to adopt the entire South-Tyrol region for the calculation of G is due to the fact that the Passirio basin, despite being ideal for representing the hydrological behaviour of snow-dominated Alpine catchment, is too small to guarantee an adequate representation of precipitation trends with elevation. A similar approach was used for setting-up ICHYMOD in the same region by Di Marco et al. (2021) and Shrestha et al. (2023).

The temperature lapse rate $LR(t)$ was evaluated at each hourly time step within ICHYMOD model itself according to the different meteorological forcing datasets and considering for each of them the values at the grid points in the Passirio catchment as a proxy for ground stations. For the sake of clarity, Fig. 3 shows an example of the evaluation of the temperature lapse rate in a generic time step t for the datasets REA11×8, KR11×8 and KR1×1. As can be seen, the higher the resolution of the dataset, the more temperature data are considered for the regression. This in turn leads to a different hourly lapse rate and therefore a potential different simulation outcomes of snow dynamics and runoff generation.

The hydrological experiments are carried out considering the classical hydrological year time spawn (October to September in the ensuing year). Specifically, the model was first calibrated, with reference to each of the three meteorological datasets, during the period from 1st October 2013 to 30th September 2017 (termed calibration period hereafter) by adopting the NSE as an efficiency metric (see Section 3.5). In the current application the parameters involved in calibration were 9 of the those outlined in Table 2 (considering G calibrated a priori, as described above in this section). For each calibration experiment the number of iterations used was 5000 and the best parameters were selected based on NSE. Furthermore, the first three years of the simulations (from 1st October 2010 to 30 September 2013) were used as a warm-up period to avoid dependence on the initial condition and therefore excluded from the computation of the model performance. Validation of the modelling framework was then performed on the period from 1st October 2017 to 30 September 2019 (termed validation period hereafter) for all three calibration experiments by computing
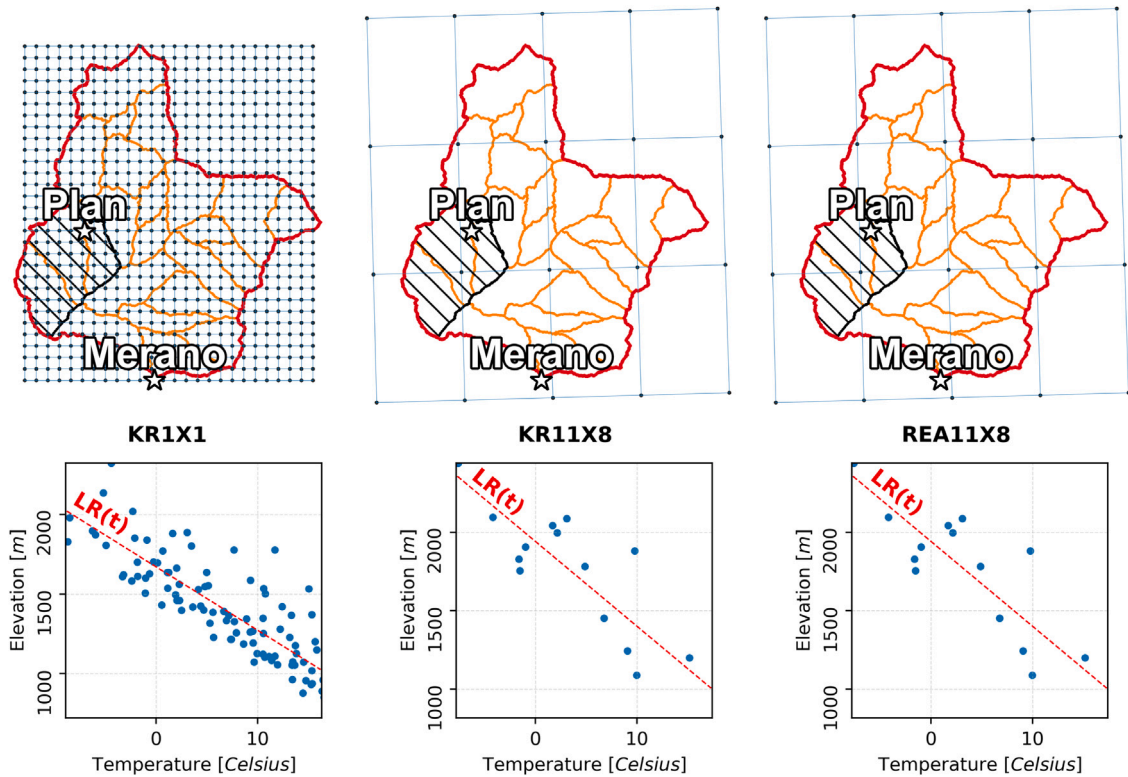
Fig. 3. In the first row the Passirio catchment closed at Merano is presented together with its 23 sub-catchments and the meteorological datasets grids covering the basin. The three dashed sub-catchments represent the nested Plan sub-catchment. In the second row, an example of evaluation of the temperature lapse rate $LR(t)$ on a generic time step t is presented with reference to the three adopted datasets.

NSE at the Merano gauging station. Moreover, the Plan gauging station was used for spatial validation by considering in this case the entire time period spanning from 1st October 2013 to 30th September 2019. This evaluation aimed to assess the hydrological framework robustness, as outlined in work (Di Marco et al., 2021), evaluating the hydrological consistency of the hourly datasets across various catchment sizes.

Simulated streamflow for the different experiments was then compared chronologically as hourly time series and by computing their Empirical Cumulative Distribution Functions (ECDFs) to identify possible biases at the different flow regimes. Furthermore, the comparison was also performed by considering the following seasonal aggregations: winter from December to February, spring from March to May, summer from June to August, and autumn from September to November. Finally, the response of the snow dynamics to the different meteorological forcing, as simulated by the cryospheric component of the ICHYMOD model, was performed to emphasize the importance of the combined role of temperature and precipitation biases.

4. Results

4.1. Creation of the gridded observational data reference dataset

According to the procedure described in Section 3.3 the 1-km gridded KR1×1 dataset was created with reference to the time window 2010–2019. At the hourly time scale, the Mean Absolute Error (MAE) and the Mean Error (ME) obtained through the cross-validation procedure are 0.07 mm (ME: 0.00 mm) for precipitation and $1.82\,°C$ (ME: $0.57\,°C$) for temperature, respectively.

Fig. 4 reports KR1×1 spatial distribution for (a) precipitation and (b) temperature aggregated at the yearly time scale. The average annual precipitation obtained over the period 2010–2019 is 921 mm, while the average monthly temperature ranges from the minimum of $-3.78\,°C$ to the maximum of $13.32\,°C$.

The Mean Absolute Error (MAE) and Mean Error (ME) metrics, aggregated on a daily basis, were obtained through the cross-validation procedure (refer to Section 3.3) and are presented in Table 4, categorized by different months. These findings align with the results reported by Crespi et al. (2021a), who recently published a high-resolution daily gridded dataset of temperature and precipitation for the Trentino/South-Tyrol region.

As observed in Table 4, the precipitation Mean Absolute Error (MAE) ranges from 0.5 mm to 1.8 mm, with more substantial errors occurring during the summer season (i.e., June to August), characterized by convective precipitation events. The daily Mean
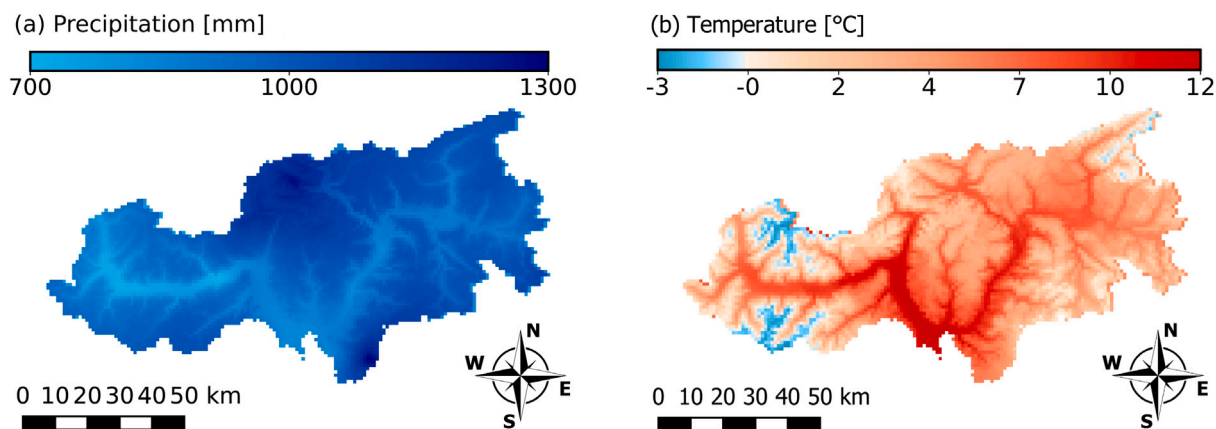
(a) Precipitation [mm]

(b) Temperature [°C]

Fig. 4. High resolution 1×1 km gridded datasets of the annual mean (a) precipitation and (b) temperature over the South-Tyrol Province during the period 2010–2019.

Table 4
Monthly cross-validation metrics across the South-Tyrol stations obtained by the kriging interpolation performed at 1 km scale. Mean Absolute Error (MAE) and Mean Error (ME) at the daily temporal resolution are reported for both precipitation and temperature variables.

	Precipitation		Temperature	
	MAE [mm]	ME [mm]	MAE [°C]	ME [°C]
January	0.5	0.0	1.6	0.0
February	0.5	0.0	1.6	0.0
March	0.5	0.0	1.6	0.0
April	0.7	0.0	2.6	0.0
May	1.2	0.0	1.6	0.1
June	1.5	0.0	1.6	0.1
July	1.8	0.0	1.5	0.1
August	1.7	0.0	1.5	0.0
September	1.0	0.0	1.5	0.0
October	1.0	0.0	1.4	0.0
November	0.9	0.0	1.4	0.0
December	0.5	0.0	1.6	0.0

Error (ME) remains consistently at $0 \, \text{mm}$ throughout the entire year, a value consistent with the findings of Crespi et al. (2021a). Regarding temperature, the MAE varies from $1.4 \, °C$ in October to $2.6 \, °C$ in April, with the ME increase to $0.1 \, °C$ in Summer while it remains consistently at $0 \, °C$ along the other seasons. Generally, lower MAE are observed in the summer and autumn seasons, while larger errors are evident in winter and spring. In this context, the cross-validation results align with those presented by Crespi et al. (2021a), reporting MAE values ranging from $1.1 \, °C$ to $1.8 \, °C$.

4.2. Comparison between meteorological forcing

The results here presented aim to analyse the biases characterizing ERA5-Land product by performing a comparison between REA11×8 and KR11×8 datasets at different spatial and temporal scales. Indeed, bias in this work is the difference between the REA11×8 and the KR11×8 datasets.

Fig. 5 compares the spatially aggregated mean of hourly REA11×8 and KR11×8 data using the Empirical Cumulative Distribution Functions (ECDFs) for temperature and using Exceedance Probability curves for precipitation, as well as their monthly aggregation displayed as boxplots. As it can be noticed from Fig. 5(a), REA11×8 exhibits higher precipitation values than KR11×8 for events below $1 \, \text{mm/h}$ with a non-zero event probability of 64% compared to 42% for KR11×8. On the other hand, KR11×8 presents larger values for exceedance probability lower than 5%. The prevalence of larger values for REA11×8 with respect to KR11×8 (i.e., a positive bias) is also confirmed by visual inspection of Fig. 5(b) where a mean bias of about $30 \, \text{mm/month}$ is observed throughout the year. Besides, the highest bias values occur in terms of monthly average between April and July, with a value around $40 \, \text{mm/month}$. The bias observed in the other months is lower with a minimum of $20 \, \text{mm/month}$ in September and an average of $30 \, \text{mm/month}$.

Regarding temperature, Fig. 5(c) highlights how REA11×8 dataset presents colder temperatures than the KR11×8 dataset, with a median positive bias of $2.1 \, °C$. The variation in temperature is minimal for higher quantiles, but as we move towards lower exceedance probability values, the difference becomes more pronounced, reaching a maximum of approximately $6 \, °C$ in the lower quantiles. The boxplots in Fig. 5(d) highlight that temperature biases are more pronounced in winter and spring compared to summer and autumn, exhibiting a clear seasonal pattern.
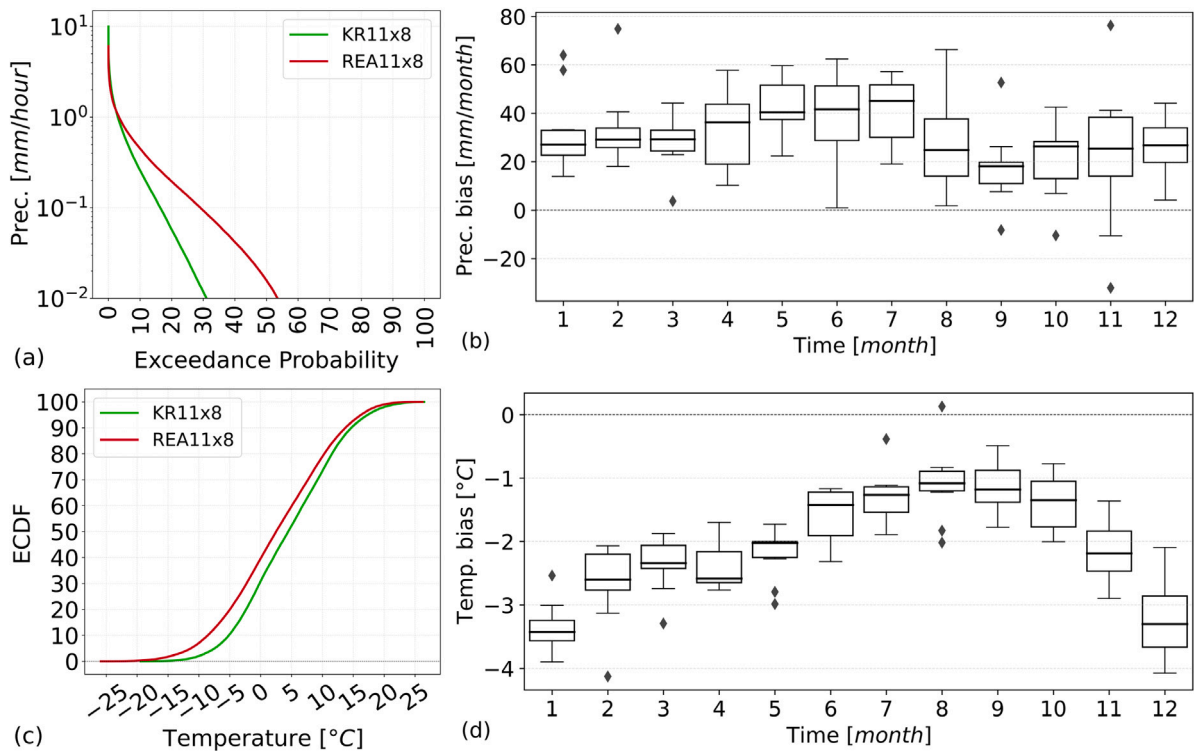
Fig. 5. Comparison between REA11×8 and KR11×8 datasets spatially aggregated over the South-Tyrol: (a) the precipitation exceedance curve of the hourly data, (b) the precipitation monthly boxplots, (c) the temperature ECDFs of the hourly data and (d) the temperature monthly boxplots.
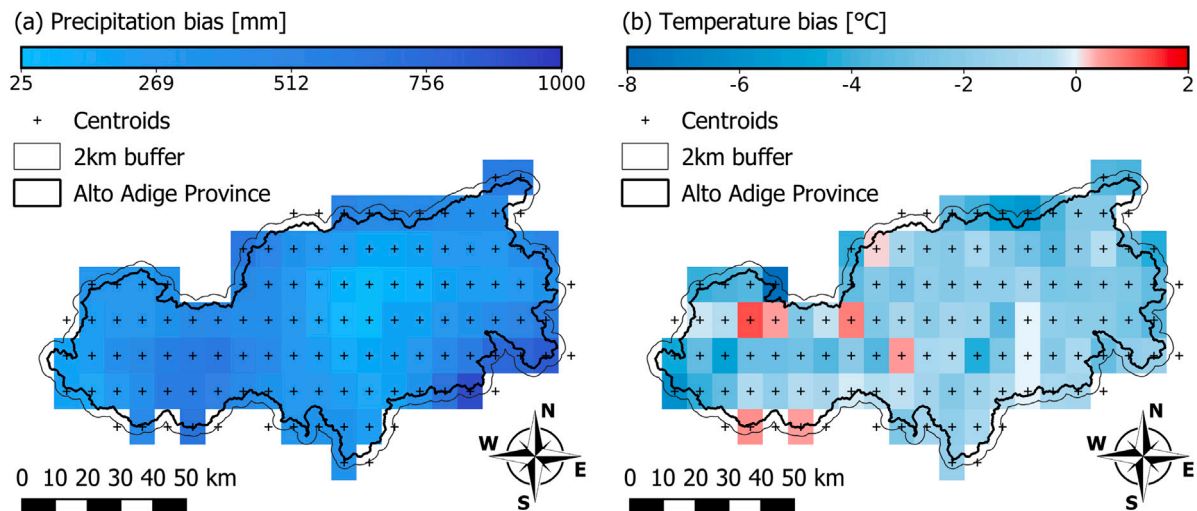

Fig. 6. Spatial distribution of the bias between REA11×8 and KR11×8 datasets aggregated at the yearly time scale for (a) precipitation and (b) temperature.

Assessment of the spatial variability of the biases is presented in Fig. 6 in terms of yearly cumulative precipitation and mean temperature differences between the two datasets, respectively. It can be noticed from Fig. 6(a) that the dissimilarity in annual precipitation ranges between $27\,\text{mm/year}$ and $915\,\text{mm/year}$ among all the cells in the region of interest. Besides, the application of a t-test provided a p-value of 0.49 highlighting how no significant correlation can be retrieved between biases and elevation.

The spatial distribution of the temperature bias is presented in Fig. 6(b). Differences ranges from a minimum of $-7.9\,°\text{C}$ to a maximum of $1.25\,°\text{C}$. Opposite to the case of precipitation, the bias presents a significant correlation with elevation as evidenced by the p-value of 0.005 obtained when applying the t-test. The identified trend between the bias and the elevation can be estimated

Table 5

Precipitation and temperature seasonal bias over South-Tyrol during the period 2010–2019.

	Precipitation	Temperature
Autumn	62.32	−1.42
Winter	90.87	−3.18
Spring	102.85	−2.19
Summer	108.69	−1.16

Table 6

Nash–Sutcliffe Efficiency indexes during the calibration (from 1st October 2013 to 30th September 2017) and validation periods (from 1st October 2017 to 30th September 2019) for the simulations conducted at the Merano gauging station. Validation during the entire observational period at Plan is also presented for the three different datasets.

Station	Merano		Plan
From	1st Oct 2013	1st Oct 2017	1st Oct 2013
To	30th Sep 2017	30th Sep 2019	30th Sep 2019
KR1×1	0.78	0.60	0.61
KR11×8	0.70	0.51	0.47
REA11×8	0.39	0.37	0.63

in about 0.5 °C per 1000 m. This result indeed shows that the bias is more noticeable at higher elevations, with the REA11×8dataset presenting colder temperatures in mountainous sub-catchments than in valleys.

Finally, Table 5 illustrates the biases in precipitation and temperature within both the REA11×8and KR11×8 datasets, aggregated seasonally and spatially. It is noteworthy that precipitation exhibits positive biases across all seasons, indicating a wetter tendency in reanalysis data compared to observational data. Conversely, temperature is characterized by negative biases throughout the year, suggesting that reanalyses depict cooler conditions than the observational datasets.

Concerning the Passirio catchment (see Fig. 1) it is noteworthy that the monthly average precipitation bias is 33.4 mm, varying between 7.58 mm in November and 67.91 mm in July. The monthly temperature bias over the same catchment averages −1.8 °C, ranging from a minimum of −3.7 °C in January to a maximum of −0.7 °C in July. Similar patterns are observed in the Plan catchment (see Fig. 1), where the monthly average precipitation bias is 36.7 mm, fluctuating between 11.28 mm in November and 77.17 mm in July. The average monthly temperature bias in the Plan catchment is −1.2 °C, with a minimum of −3.3 °C in January and a maximum of 0.2 °C in July.

4.3. Hydrological model simulations and coherence

Table 6 shows the NSE coefficients of the hydrological calibrations performed with the three datasets KR1×1, KR11×8 or REA11×8used as input meteorological forcing. The adoption of the higher resolution KR1×1dataset leads to a value of NSE equal to 0.78 during the calibration period at the Merano station. On the other hand, the upscaled observational dataset KR11×8 leads instead to a slightly lower value of 0.70 always evaluated at the Merano gauging stations. The simulations conducted during the validation period present a small deterioration of the performances with NSE equalling 0.60 for KR1×1 and 0.51 for KR11×8, respectively. It is worth mentioning that the NSE values during validation are greater than 0.5 and therefore simulations can be considered acceptable following the classification introduced by Moriasi et al. (2007). On the contrary, the adoption of the REA11×8dataset results in not satisfactory hydrological model performances at Merano, with a value of NSE equalling 0.39 in calibration and 0.36 in validation, respectively.

Spatial validation of the hydrological modelling was also performed by simulating streamflow at the Plan gauging station (see Fig. 9). Concerning the observational datasets, the efficiency metrics show a decline in performance with values of NSE equalling 0.61 and 0.47 for KR1×1 and KR11×8, respectively, still close to the acceptability threshold for the latter case. On the contrary, the adoption of the reanalysis dataset REA11×8leads to a value of NSE equalling 0.63, slightly better than the value obtained at Plan with the observational dataset KR1×1. Surprisingly, this result entails not only a satisfactory reproduction of the observed streamflow at the validation site but also a significant increment of the modelling performances with respect to the calibration experiment. This latter and counterintuitive aspect will be further discussed in Section 5.

Figs. 7 and 8 provide further insights into hydrological simulation outcomes. On one hand, Fig. 7 shows the ECDFs of the simulated flows against the observed streamflows at Merano station during the calibration (subplot a) and the validation (subplot b) periods, respectively. As can be noticed, the gridded observational datasets (KR1×1 and KR11×8) exhibit similar behaviour on the entire Passirio during both periods, whereas the REA11×8always overestimates observed streamflows (black lines in Fig. 7a and b). The mean streamflow metered at the Merano gauging station is 11.60 m^3/h during the calibration period, a value which is well reproduced by simulations conducted with KR1×1 and KR11×8 datasets which present mean streamflow of 11.70 m^3/h and 11.66 m^3/h, respectively. On the contrary, simulations conducted using REA11×8as forcing lead to a significant overestimation of mean streamflow which equals 16.22 m^3/h. In addition, overestimation of the streamflow occurs for 90 % of the simulation time steps as depicted in both plots of Fig. 7.
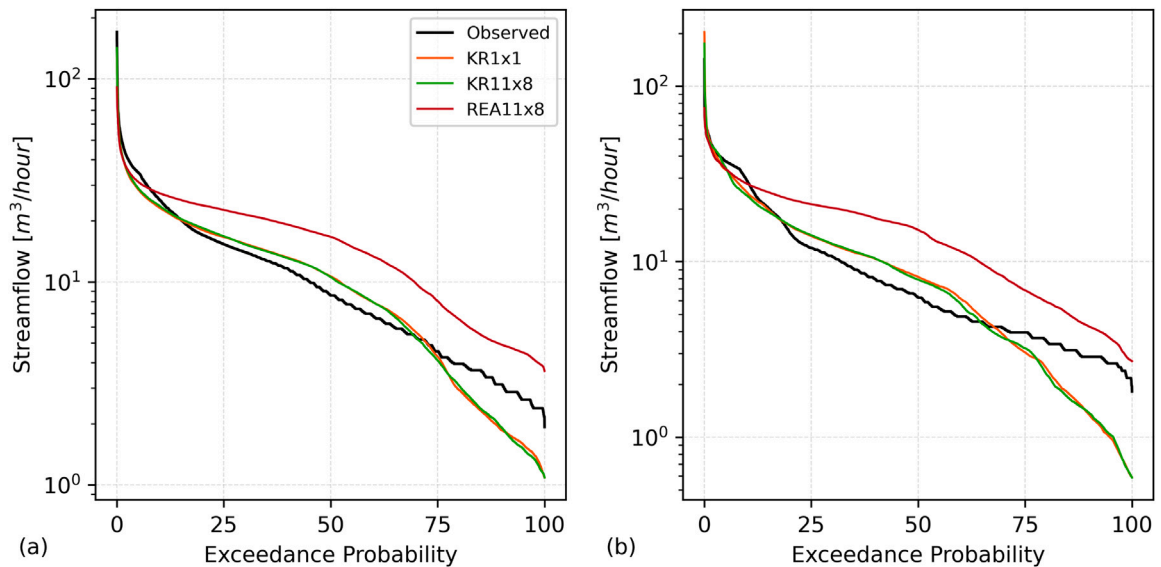
Fig. 7. Streamflow over Passirio catchment at the Merano gauging station: exceedance curves at hourly resolution for (a) the calibration and (b) the validation periods, respectively.
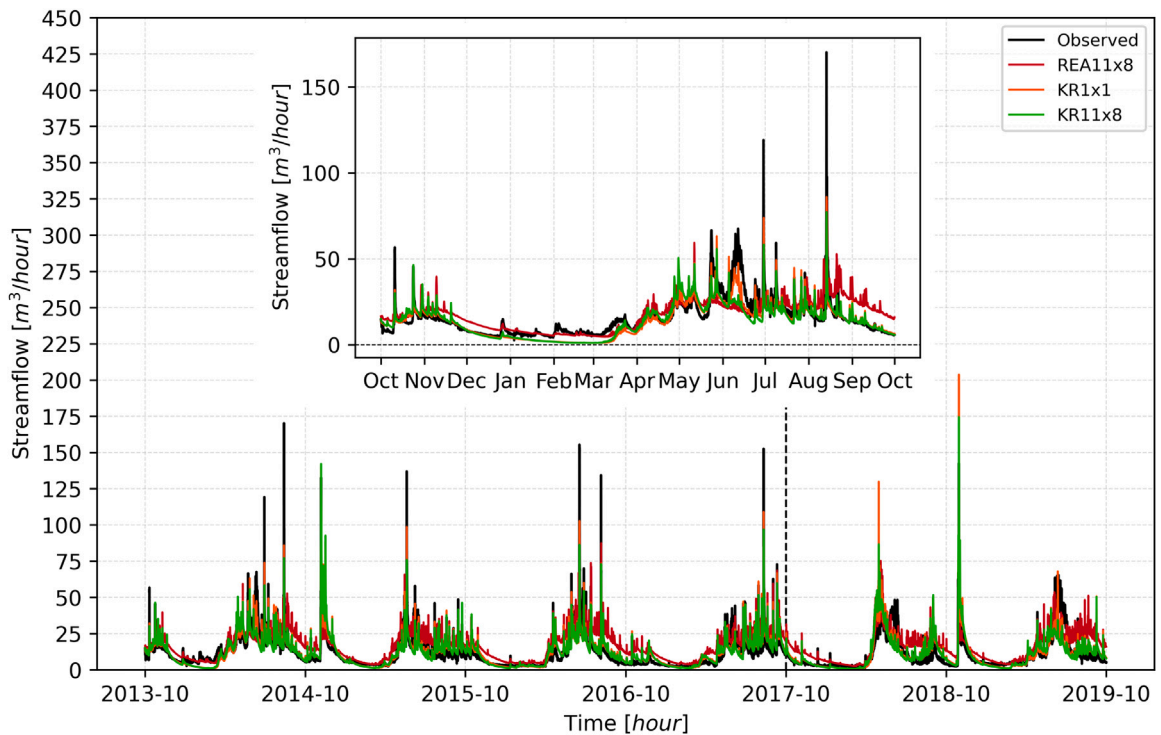

Fig. 8. Hourly streamflow time series in the Passirio catchment at the Merano gauging station during the entire observational period 1st October 2013–30th September 2019. The inset shows a focus on the hydrological year spanning from 1st October 2014 to 30th September 2015.

On the other hand, Fig. 8 compares the time series of observations measured at Merano gauging station with the simulations obtained by using as input the three different datasets. All the simulations are generally capable of reproducing the observed streamflow timing. In addition, and in agreement with the results presented in Fig. 7, simulations conducted with REA11×8 present a significant overestimation of the observed streamflow, particularly evident during the recession limbs of the hydrograph. On the contrary, KR1×1 and KR11×8 exhibit a small underestimation of observations under baseflow conditions. These differences are even
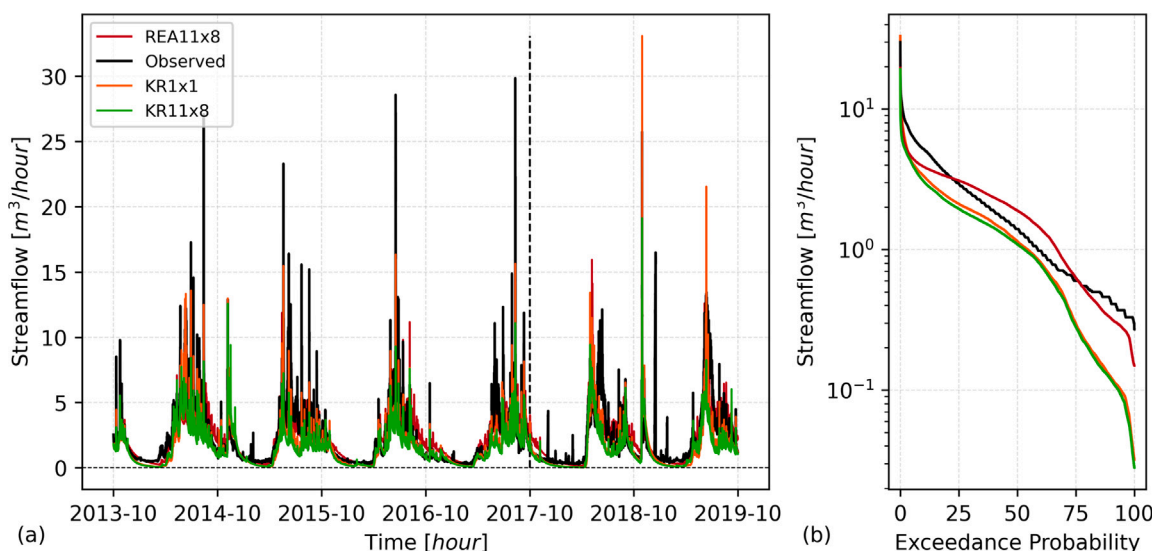
Fig. 9. Hourly streamflow time series at the Plan sub-catchment: (a) chronological comparison and (b) exceedance curves during the entire observational period 1st October 2013–30th September 2019.

more evident when focusing solely on the hydrological year spanning from 1st October 2014 to 30th September 2015, as shown in the inset of Fig. 8.

In addition, the inset of Fig. 8 allows an improved visual representation of the overall streamflow overestimation obtained when using REA11×8dataset. The inset also emphasizes how both KR1×1 and KR11×8 forced simulations exhibit similar results, with KR1×1 performing slightly better in reproducing observed streamflow during the spring and summer seasons, and both simulations slightly underestimating baseflow during the winter season. Comparatively, the simulation using the REA11×8dataset yields slightly worse results than KR11×8 in autumn and summer. Additional discussion of these seasonal differences is reported in Section 5.3.

Fig. 9(a) compares observed and simulated streamflow time series during the overall observational period at the Plan gauging station, used for spatial validation. Still at Plan, Fig. 9(b) shows the exceedance curves during the same period. The latter, in particular, highlights how simulations conducted using KR1×1 and KR11×8 datasets always slightly underestimate observed streamflow, with KR1×1 providing a better representation than KR11×8 of the lowest quantiles (i.e., high streamflow events). Contrary to the case of Merano, simulation with REA11×8provides slightly better results than both kriging-based simulations, with, in particular, a better representation of the baseflow and of the melting season. Further discussion on these seasonal differences is reported in Section 5.

5. Discussion

5.1. High-resolution interpolated dataset

The results presented in Section 4.1 exhibit consistency with existing literature regarding precipitation and temperature for the investigated region. Specifically, the KR1×1 dataset aligns closely with findings from Laiti et al. (2018), which reported an average annual precipitation ranging between 883 mm and 1052 mm based on five distinct datasets (E-OBS Cornes et al., 2018, MSWEP Beck et al., 2018, MESAN Landelius et al., 2016, APGD Isotta and Frei, 2013, and ADIGE Mallucci et al., 2019). Additionally, the KR1×1 dataset, with an annual mean temperature of 6.2 °C, corresponds closely with Lutz et al. (2016), which report an annual mean temperature of 3 °C for the Adige basin over the period 1961–1990. Similarly, Crespi et al. (2021a) documented a temperature of 5 °C for the Trentino/South-Tyrol region during the period 1981–2010.

It is worth to mention that KR1×1 is the only dataset providing hourly temporal resolution for the entire Alpine region to the best of the author's knowledge.

It is important to underline that the adoption of the Kriging as an interpolation scheme has a key advantage: Kriging is indeed an exact interpolator and it is recognized as one of the best linear unbiased estimators (Goovaerts, 1997; Eldeiry, 2012). This means that, unlike other interpolators, such as least squares polynomial fitting (Gentile et al., 2012) or linear regression (Crespi et al., 2021a), the interpolated value at a sample location is equal to the observed value at that location, while the prediction error is minimized and has a zero mean (Goovaerts, 1997). As all interpolators also kriging has some drawbacks, which may be enhanced in alpine regions. It is indeed sensitive to the size and spatial distribution of the observations and to the spatial auto-correlation of the data. As a consequence, either sparse sampling or clustering of weather stations could lead to suboptimal reconstruction of both precipitation and temperature fields. This is indeed not the case in our study where the station network is fairly dense and well distributed over the investigated domain shown in Fig. 1.

Table 7

Hourly cross-validation errors averaged across the South-Tyrol station for precipitation and temperature variables.

	Precipitation	Temperature
Elev. band [*m.a.s.l.*]	MAE [mm]	MAE [°C]
From 0 to 1000	0.058	1.69
From 1000 to 1800	0.072	1.29
Over 1800	0.088	1.44

Instrument type, site elevation, and exposure of weather stations are other sources of uncertainty that may affect the accuracy of the kriging interpolation performed in this study, as well as that which would have been obtained using different schemes (Nijssen and Lettenmaier, 2004; Tian et al., 2013). Besides, *rain gauge undercatch* is another well-known source of error in precipitation records, particularly at high altitudes. This can indeed account for up to several tens of percent of the measured precipitation value (Frei and Schär, 1998), while different shelters of the weather station from direct sunlight affect the instrumental temperature recording (Böhm et al., 2010). Our results are in line with those findings as further highlighted in Table 7 which reports the hourly MAE for both precipitation and temperature over three elevation bands: from 0 m a.m.s.l. to 1000 m a.m.s.l., from 1000 m a.m.s.l. to 1800 m a.m.s.l. and over 1800 m a.m.s.l.. It can be noticed that the MAE of precipitation increases with elevation, whereas the MAE of temperature presents the lowest values at the higher elevations. Conversely, no discernible trend exists between elevation and temperature errors.

In general, interpolation methods like kriging can greatly benefit from incorporating external information, such as radar data, which aids in better understanding extreme events and filling spatial gaps. While these methods have demonstrated good performance in Alpine regions (Rysman et al., 2016; Sideris et al., 2014), they are tailored only for precipitation estimation and can introduce complexity to data management. Further analysis is required to extend these findings to our specific case study area. Nonetheless, our investigation indicates that kriging yields strong outcomes in this region, as detailed in Section 4.1.

5.2. Comparison between ERA5-Land and the interpolated datasets

5.2.1. Precipitation

The significant precipitation overestimation by ERA5 reanalysis dataset with respect to the observational dataset generated by means of kriging interpolation is consistent with the recent findings by Bandhauer et al. (2022), which showed that ERA5 overestimates precipitation in three European sub-regions characterized by prominent mountain ridges, namely an Alpine, a Carpathian and a Fennoscandian transect. Similarly, Amjad et al. (2020) showed that both ERA-Interim and ERA5 have a wet bias with respect to observations in the mountainous region of Turkey.

In our case study, the significant differences between ERA5-Land and KR11×8 can be attributed to two different factors: (i) a possible precipitation undercatch by KR11×8, the effect which may be relevant in alpine regions and at high altitudes; and (ii) the significant overestimation by ERA5-Land of the frequency of wet days over the Alps (up to a factor of 2), as also reported in Bandhauer et al. (2022) and Monteiro and Morin (2023).

5.2.2. Temperature

The seasonal variability of temperature biases, as depicted in Fig. 5 for the entire South-Tyrol region, corresponds to patterns observed in the French Alps (Monteiro et al., 2022) and the broader European Alps (Monteiro and Morin, 2023). Notably, the most significant disparities between reanalysis and observational datasets manifest during the winter months (see Fig. 5(d)). It is noteworthy that a similar bias pattern in ERA5-Land temperature was also identified by Huang et al. (2022) in the Qinghai-Tibet Plateau concerning both in-situ observations and the US Global Land Data Assimilation System (GLDAS).

Additional factors, including elevation, aspect, slope, vegetation, and snow cover, each entangled within intricate interdependencies, may contribute to the diverse capacity of the reanalysis product in replicating observations throughout the year (Hersbach et al., 2020). Specifically, the discerned dependency of temperature biases on elevation, as unveiled through the application of the t-test outlined in Section 3.6, resonates with findings presented by Monteiro and Morin (2023) for the European Alps. Moreover, a distinct bias pattern is evident throughout the year (refer to Table 5), aligning with Monteiro and Morin (2023), who reports peak biases in December and January, ranging between −2 °C and −3.5 °C from November to February. It is pertinent to acknowledge that disparities may stem from variations in the analysed period and geographical region.

5.3. Testing the hydrological coherence

Hydrological coherence of the climate datasets is assessed according to their ability to reproduce the observed streamflow time series, following the HyCoT methodology described in Section 3.5.

Hydrological simulations conducted using the two observational gridded datasets (i.e., KR1×1 and KR11×8) characterized by a different spatial resolution showed no significant differences at Merano gauging station. This finding is consistent with previous studies (Nicòtina et al., 2008; Ghimire et al., 2022; Volpi et al., 2012; Michelon et al., 2021) showing that for medium to large watersheds, the total rainfall amount is more important than the spatial distribution of rainfall for an accurate reproduction of the
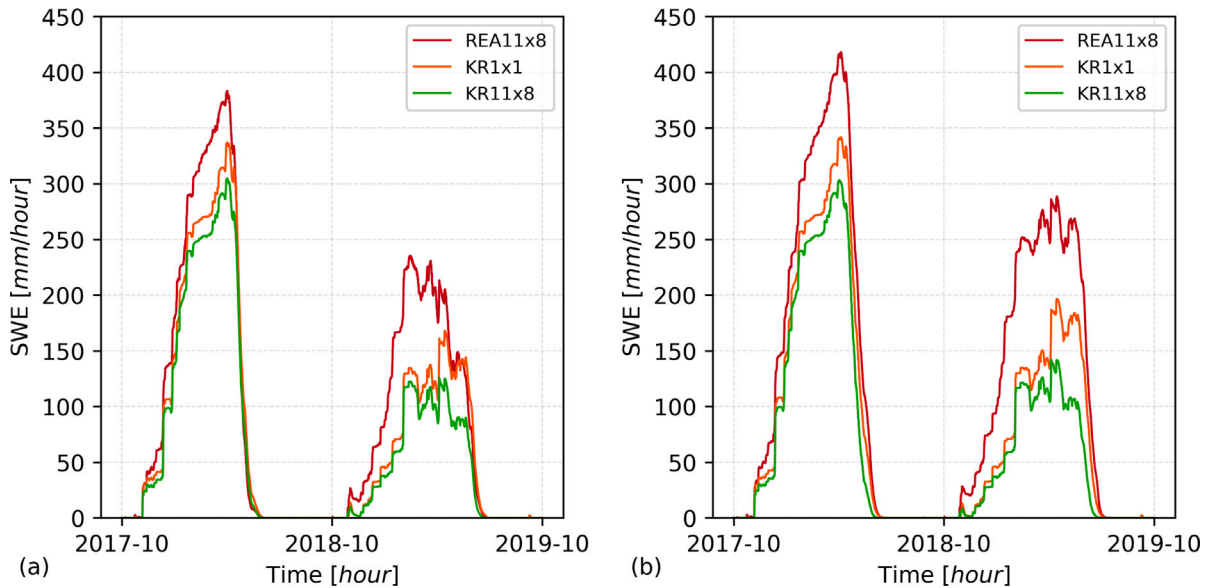
Fig. 10. SWE comparison of the three datasets simulations: (a) on Passirio and (b) on Plan catchment, both during the validation period from 1st October 2017 to 30th September 2019.

observed hydrographs. This is also coherent with the poor performances of the simulations conducted by using ERA5-Land as the input, where the significant precipitation overestimation in comparison to observational datasets led to a significant bias of the simulated streamflows.

The results obtained by spatial validation at the Plan station, a small nested sub-catchment of the Passirio (see Fig. 1) involve a more complex interpretation. On the one hand, the use of the higher spatial resolution dataset (KR1×1) is associated with improved performances with respect to the coarser dataset (KR11×8). On the other hand, an unexpected improvement in performance results from the use of ERA5-Land. In this case, we argue that the hydrological response in this small snow-dominated Alpine catchment is shaped not only by the spatial pattern of precipitation but also, and to a major extent, by the interplay of temperature and precipitation in controlling snowmelt dynamics, as also highlighted in Zhang et al. (2015), Girons Lopez et al. (2020) and Ruelland (2020).

Modelling of snow dynamics is, therefore, of paramount importance to assess the reliability of ERA5-Land in hydrologic simulations performed in high-altitude headwaters. To this end, we analysed the Snow Water Equivalent (SWE) simulated by the model using the three different meteorological forcing datasets (i.e., KR1×1, KR11×8, and REA11×8) in both the entire Passirio and the Plan catchments during the validation period. This comparison is depicted in Fig. 10, which shows clearly how the simulation driven by reanalysis (REA11×8) results in greater SWE for both basins with respect to those obtained by using the observational datasets (i.e KR1×1, KR11×8). This can be attributed to the pronounced positive precipitation bias in winter, resulting in larger available water volumes, which coupled with the colder temperatures of ERA5-Land leads to significantly larger values of SWE. This latter result is also confirmed by the recent work of Shrestha et al. (2023) where the use of ERA5 as input forcing for SWE simulations in Alpine basins resulted in an overestimation not only of SWE but also of the snow-cover area in the upper part of the Adige basin.

The significant differences in simulating the temporal evolution of SWE among the three datasets are also witnessed by the different values of the TOPMELT snow module parameters obtained during calibration as presented in Table 8. Firstly, the precipitation lapse rate G is similar for KR1×1 and REA11×8, but it is significantly lower for KR11×8. Therefore, it appears that ERA5-Land captures the precipitation orographic enhancement due to elevation, a widely acknowledged phenomenon in the alpine region (e.g. Avanzi et al. (2021)), as effectively as the high-resolution observation dataset (i.e. KR1×1). Secondly, the large value of the Melt Factor (CMF) obtained for REA11×8case indicates that the calibration process tries to compensate for the negative ERA5-Land temperature biases in order to ensure the correct streamflow simulation at Merano gauging station. As it can be noticed from Eq. (4), the larger the value of CMF the larger is the snowmelting occurring at lower temperatures thus compensating for the colder values of REA11×8if compared with those of KR1×1 and KR11×8 observational datasets. The same compensation occurs, although to a lesser extent, for the Fresh Snow Albedo (alb_s) parameter, which dwindles moving from the observational datasets-driven calibrations to the case in which REA11×8is used. Notice that a reduction in the snow albedo is associated to a larger share of input radiation into the snowpack and thus to enhanced snow melting. The Rain Melt Factor RMF deserves instead a separate discussion. This refers indeed to the rain-on-snow conditions where melting depends on both precipitation and temperature. The

Table 8

TOPMELT snow module calibrated parameters for the three different experimental setups, corresponding to the three different forcing used (i.e., KR1×1, KR11×8 and REA11×8). The description of each parameter is reported in Section 3.4.

Name	Unit	KR1×1	KR11×8	REA11×8
CMF	$\frac{mm\,m^2}{MJ\,h\,°C}$	0.0025	0.0025	0.008
G	$\frac{mm}{km}$	0.064	0.019	0.076
alb_s	–	0.85	0.96	0.77
RMF	$\frac{1}{h\,°C}$	0.07	0.03	0.025

interplay between these two factors seems more correlated to the different resolution of the datasets, with similar values obtained in calibration for KR11×8 and REA11×8and a larger value obtained for KR1×1. This behaviour could be attributed to the fact that the coarse resolution results in the averaging of temperature and precipitation, which affects the rain-on-snow cusp conditions.

To complete the discussion of the hydrological performance, seasonal streamflows are reported as exceedance curves in Fig. 11 for both Merano and Plan gauging stations, respectively, with reference to the validation period.

Visual inspection of Fig. 11 clearly highlights how the use of REA11×8generally leads to a significant overestimation, with respect to the other datasets, of the streamflow over all the seasons and for both catchments. Indeed, overestimation by REA11×8is always present at Merano, mainly in autumn (Fig. 11(a.1)) and summer (Fig. 11(a.4)), as a consequence of the large positive precipitation biases observed in these seasons. Overestimation is also present in winter (Fig. 11(a.2)) and spring (Fig. 11(a.3)) seasons, though to a lesser extent. On the other hand, at Plan sub-catchment, REA11×8is capable of better reproducing observed streamflows in winter (Fig. 11(b.2)) and spring (Fig. 11(b.3)) with consequent lower errors in summer (Fig. 11(b.4)) as a consequence of the improved representation of snowmelt and accumulation in the preceding seasons. The role exerted by temperature in this sub-catchment is indeed highly relevant, with the cooler temperature of REA11×8with respect to KR11X8 and KR1X1 leading to a better representation of the snow-dominated seasons. This latter effect compensates for the model deficiency in reproducing reliably baseflows with REA11×8, condition which is particularly evident in autumn and summer (see the high quantiles in Fig. 11(b.1) and (b.4)). Furthermore, the impact of precipitation undercatchment at Plan, evident in both KR1×1 and KR11×8 datasets, is particularly notable during winter and spring (refer to Fig. 11(b.2) and (b.3)). Consistent with the findings of Collados-Lara et al. (2018), undercatchment of precipitation at high elevations significantly influences the outcomes of the snow melting module. In summary, our results affirm the substantial role of precipitation volume in shaping streamflow responses in medium to large catchments, with temperature gaining heightened significance in smaller, high-elevation catchments.

The use of KR1×1 leads to better performances than KR11×8, as also shown by NSE indexes presented in Table 6. The differences are associated in this case with the different spatial resolution which entails a significantly different evaluation of the temperature lapse rate at each time step (see Section 3.6).

6. Conclusion

This study highlights the need to rely on accurate and high-resolved in space and time meteorological data for hydrological applications, particularly in the context of the Alpine Region. Hydrological models are essential for various applications, including flood risk assessment, hydropower production, and water management. However, the reliability of these models hinges on the spatial and temporal representation of meteorological forcing data, which can significantly impact the simulation of key hydrological processes such as snow accumulation and melt.

Given some limitations (e.g. undercatchment) of in-situ meteorological stations and their declining numbers, this study explores the use of ERA5-Land climate reanalyses dataset, which offers promising possibilities by providing meteorological data with no gaps over extended time periods and domains. However, its suitability for hydrological modelling in the Alpine Region remains to be thoroughly assessed. To achieve this, the study focuses on the South-Tyrol region and the Passirio catchment as representative examples. By developing high-resolution observational datasets and comparing them with ERA5-Land datasets, the research aimed at evaluating the biases in temperature and precipitation and assessed the suitability of ERA5-Land for hydrological modelling. The Hydrological Coherence Test (HyCoT) is employed to evaluate the hydrological coherence of these datasets with streamflow observations, shedding light on their effectiveness in improving hydrological simulations in snow-dominated Alpine catchments. Furthermore, the creation of a novel 1 km spatial resolution dataset by means of kriging with external drift algorithm offers a valuable benchmark for future hydrological studies in the region.

Despite its undisputed relevance, the presence of significant precipitation and temperature biases in the ERA5-Land dataset propagates throughout the hydrological modelling chain and significantly deteriorates the accuracy of hydrological simulations, particularly at medium spatial scales. In this sense, a possible solution could be to correct the bias of the ERA5-Land meteorological forcing to improve hydrological performance, by implementing bias adjustment methods typically used in climatological impact studies. Further research along this line is currently under development.
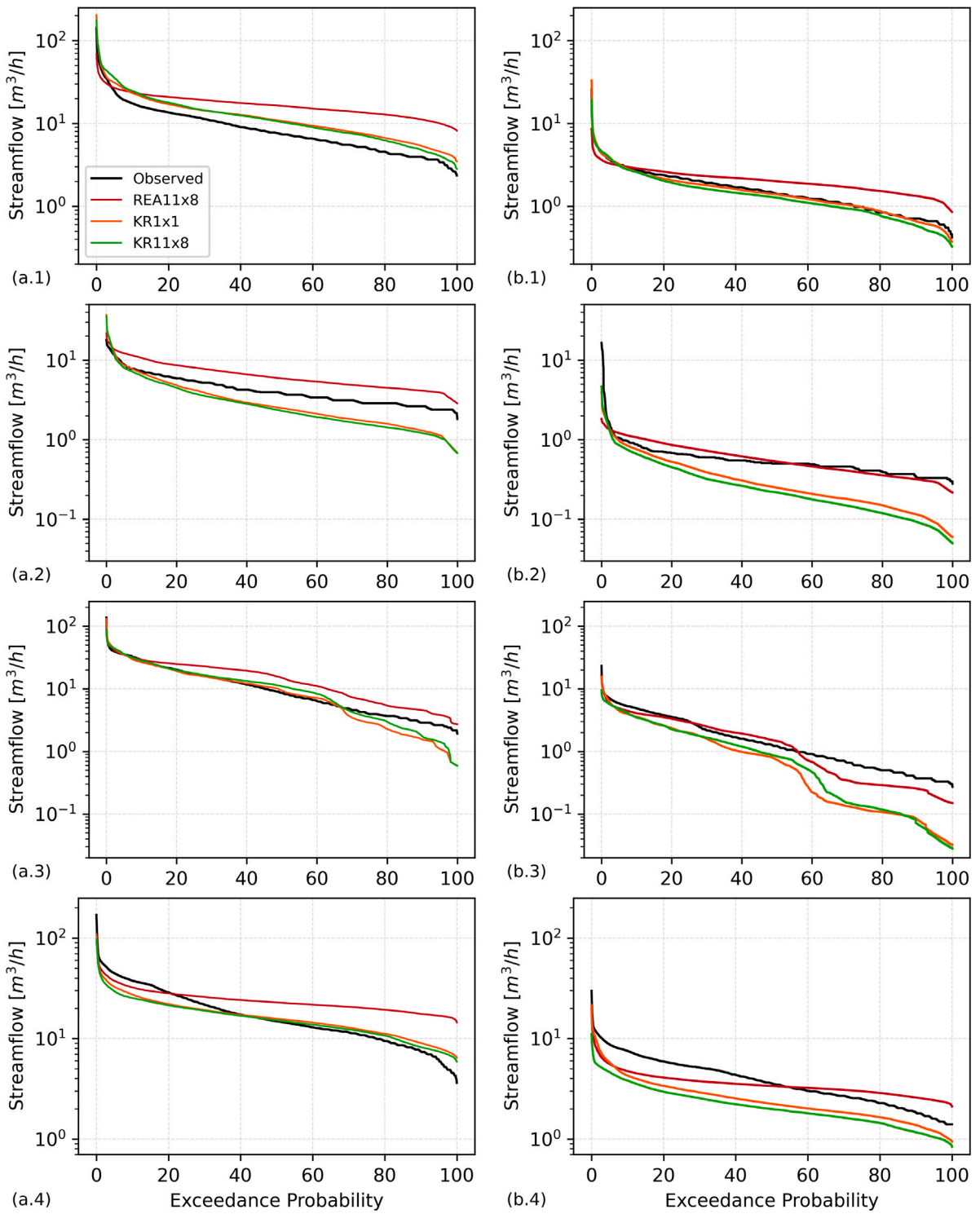
Fig. 11. Exceedance curves of the seasonal streamflow (1:autumn, 2:winter, 3:spring, 4:summer) at Merano (a.1)–(a.4) and Plan (b.1)–(b.4) gauging stations.

CRediT authorship contribution statement

Declaration of competing interest

The authors declare that they have no known competing financial interests or personal relationships that could have appeared to influence the work reported in this paper.

Data availability

The manuscript contains the link where to download the data.

Acknowledgements

References

Amjad, M., Yilmaz, M.T., Yucel, I., Yilmaz, K.K., 2020. Performance evaluation of satellite- and model-based precipitation products over varying climate and complex topography. J. Hydrol. 584, 124707. http://dx.doi.org/10.1016/j.jhydrol.2020.124707, URL: https://www.sciencedirect.com/science/article/pii/S0022169420301670.

Apel, H., Thieken, A.H., Merz, B., Blöschl, G., 2004. Flood risk assessment and associated uncertainty. Nat. Hazards Earth Syst. Sci. 4 (2), 295–308. http://dx.doi.org/10.5194/nhess-4-295-2004, URL: https://nhess.copernicus.org/articles/4/295/2004/.

Arsenault, R., Brissette, F., 2014. Determining the optimal spatial distribution of weather station networks for hydrological modeling purposes using RCM datasets: An experimental approach. J. Hydrometeorol. 15 (1), 517–526. http://dx.doi.org/10.1175/JHM-D-13-088.1, URL: https://journals.ametsoc.org/view/journals/hydr/15/1/jhm-d-13-088_1.xml. Publisher: American Meteorological Society Section: Journal of Hydrometeorology.

Asong, Z.E., Elshamy, M.E., Princz, D., Wheater, H.S., Pomeroy, J.W., Pietroniro, A., Cannon, A., 2020. High-resolution meteorological forcing data for hydrological modelling and climate change impact analysis in the Mackenzie River Basin. Earth Syst. Sci. Data 12 (1), 629–645. http://dx.doi.org/10.5194/essd-12-629-2020, URL: https://essd.copernicus.org/articles/12/629/2020/.

Autorità di Bacino Nazionale del Fiume Adige, 2008. Bilancio idrico nel bacino dell' Adige (Quaderno).

Avanzi, F., Ercolani, G., Gabellani, S., Cremonese, E., Pogliotti, P., Filippa, G., Morra di Cella, U., Ratto, S., Stevenin, H., Cauduro, M., Juglair, S., 2021. Learning about precipitation lapse rates from snow course data improves water balance modeling. Hydrol. Earth Syst. Sci. 25 (4), 2109–2131. http://dx.doi.org/10.5194/hess-25-2109-2021, URL: https://hess.copernicus.org/articles/25/2109/2021/.

Avesani, D., Galletti, A., Piccolroaz, S., Bellin, A., Majone, B., 2021. A dual-layer MPI continuous large-scale hydrological model including Human Systems. Environ. Model. Softw. 139, 105003. http://dx.doi.org/10.1016/j.envsoft.2021.105003, URL: https://www.sciencedirect.com/science/article/pii/S1364815221000463.

Avesani, D., Zanfei, A., Di Marco, N., Galletti, A., Ravazzolo, F., Righetti, M., Majone, B., 2022. Short-term hydropower optimization driven by innovative time-adapting econometric model. Appl. Energy 310, 118510. http://dx.doi.org/10.1016/j.apenergy.2021.118510, URL: https://www.sciencedirect.com/science/article/pii/S0306261921017244.

Bandhauer, M., Isotta, F., Lakatos, M., Lussana, C., Båserud, L., Izsák, B., Szentes, O., Tveito, O., Frei, C., 2022. Evaluation of daily precipitation analyses in E-OBS (v19.0e) and ERA5 by comparison to regional high-resolution datasets in European regions. Int. J. Climatol. 42 (2), 727–747. http://dx.doi.org/10.1002/joc.7269.

Barendrecht, M.H., Viglione, A., Blöschl, G., 2017. A dynamic framework for flood risk. Water Secur. 1, 3–11. http://dx.doi.org/10.1016/j.wasec.2017.02.001, URL: https://www.sciencedirect.com/science/article/pii/S2468312416300232.

Beck, H.E., Wood, E.F., McVicar, T.R., Zambrano-Bigiarini, M., Alvarez-Garreton, C., Baez-Villanueva, O.M., Sheffield, J., Karger, D.N., 2020. Bias correction of global high-resolution precipitation climatologies using streamflow observations from 9372 catchments. J. Clim. 33 (4), 1299–1315. http://dx.doi.org/10.1175/JCLI-D-19-0332.1, URL: https://journals.ametsoc.org/view/journals/clim/33/4/jcli-d-19-0332.1.xml. Publisher: American Meteorological Society Section: Journal of Climate.

Beck, H., Wood, E., Pan, M., Fisher, C., Miralles, D., van Dijk, A., McVicar, T., Adler, R., 2018. MSWEP V2 global 3-hourly 0.1° precipitation: Methodology and quantitative assessment. Bull. Am. Meteorol. Soc. 100, http://dx.doi.org/10.1175/BAMS-D-17-0138.1.

Bellin, A., Majone, B., Cainelli, O., Alberici, D., Villa, F., 2016. A continuous coupled hydrological and water resources management model. Environ. Model. Softw. 75, 176–192. http://dx.doi.org/10.1016/j.envsoft.2015.10.013, URL: https://www.sciencedirect.com/science/article/pii/S1364815215300712.

Beven, K., Binley, A., 1992. The future of distributed models: Model calibration and uncertainty prediction. Hydrol. Process. 6 (3), 279–298.

Bisselink, B., Zambrano-Bigiarini, M., Burek, P., de Roo, A., 2016. Assessing the role of uncertain precipitation estimates on the robustness of hydrological model parameters under highly variable climate conditions. J. Hydrol.: Reg. Stud. 8, 112–129. http://dx.doi.org/10.1016/j.ejrh.2016.09.003, URL: https://www.sciencedirect.com/science/article/pii/S2214581816300817.

Böhm, R., Jones, P.D., Hiebl, J., Frank, D., Brunetti, M., Maugeri, M., 2010. The early instrumental warm-bias: a solution for long central European temperature series 1760–2007. Clim. Change 101 (1), 41–67. http://dx.doi.org/10.1007/s10584-009-9649-4.

Chiogna, G., Majone, B., Cano Paoli, K., Diamantini, E., Stella, E., Mallucci, S., Lencioni, V., Zandonai, F., Bellin, A., 2016. A review of hydrological and chemical stressors in the Adige catchment and its ecological status. Sci. Total Environ. 540, 429–443. http://dx.doi.org/10.1016/j.scitotenv.2015.06.149, URL: https://www.sciencedirect.com/science/article/pii/S0048969715303430.

Citterio, M., van As, D., Ahlstrøm, A., Andersen, M., Andersen, S., Box, J., Charalampidis, C., Colgan, W., Fausto, R., Nielsen, S., Veicherts, M., 2015. Automatic weather stations for basic and applied glaciological research. Geol. Surv. Den. Greenl. Bull. 33, 69–72. http://dx.doi.org/10.34194/geusb.v33.4512.

Collados-Lara, A.-J., Pardo-Igúzquiza, E., Pulido-Velazquez, D., Jiménez-Sánchez, J., 2018. Precipitation fields in an alpine Mediterranean catchment: Inversion of precipitation gradient with elevation or undercatch of snowfall? Int. J. Climatol. 38 (9), 3565–3578. http://dx.doi.org/10.1002/joc.5517, URL: https://onlinelibrary.wiley.com/doi/abs/10.1002/joc.5517. _eprint: https://onlinelibrary.wiley.com/doi/pdf/10.1002/joc.5517.

Copernicus Climate Change Service, E., 2019. ERA5-Land hourly data from 2001 to present. http://dx.doi.org/10.24381/CDS.E2161BAC, URL: https://cds.climate.copernicus.eu/doi/10.24381/cds.e2161bac. Type: dataset.

Cornes, R.C., van der Schrier, G., van den Besselaar, E.J.M., Jones, P.D., 2018. An ensemble version of the E-OBS temperature and precipitation data sets. J. Geophys. Res.: Atmos. 123 (17), 9391–9409. http://dx.doi.org/10.1029/2017JD028200.

Crespi, A., Matiu, M., Bertoldi, G., Petitta, M., Zebisch, M., 2021a. A high-resolution gridded dataset of daily temperature and precipitation records (1980–2018) for Trentino – South Tyrol (north-eastern Italian Alps). Earth Syst. Sci. Data Discuss. 1–27. http://dx.doi.org/10.5194/essd-2020-346, URL: https://essd.copernicus.org/preprints/essd-2020-346/. Publisher: Copernicus GmbH.

Crespi, A., Petitta, M., Marson, P., Viel, C., Grigis, L., 2021b. Verification and bias adjustment of ecmwf seas5 seasonal forecasts over europe for climate service applications. Climate 9 (12), http://dx.doi.org/10.3390/cli9120181.

Cunge, J., 2010. On the subject of a flood propagation computation method (Musklngum method). J. Hydraul. Res. April 1969, 205–230. http://dx.doi.org/10.1080/00221686909500264.

Devia, G.K., Ganasri, B.P., Dwarakish, G.S., 2015. A review on hydrological models. Aquat. Procedia 4, 1001–1007. http://dx.doi.org/10.1016/j.aqpro.2015.02.126, URL: https://www.sciencedirect.com/science/article/pii/S2214241X15001273.

Di Marco, N., Avesani, D., Righetti, M., Zaramella, M., Majone, B., Borga, M., 2021. Reducing hydrological modelling uncertainty by using MODIS snow cover data and a topography-based distribution function snowmelt model. J. Hydrol. 599, 126020. http://dx.doi.org/10.1016/j.jhydrol.2021.126020, URL: https://www.sciencedirect.com/science/article/pii/S0022169421000676.

Di Marco, N., Righetti, M., Avesani, D., Zaramella, M., Notarnicola, C., Borga, M., 2020. Comparison of MODIS and model-derived snow-covered areas: Impact of land use and solar illumination conditions. Geosciences 10 (4), http://dx.doi.org/10.3390/geosciences10040134, URL: https://www.mdpi.com/2076-3263/10/4/134.

Diamantini, E., Lutz, S.R., Mallucci, S., Majone, B., Merz, R., Bellin, A., 2018. Driver detection of water quality trends in three large European river basins. Sci. Total Environ. 612, 49–62. http://dx.doi.org/10.1016/j.scitotenv.2017.08.172, URL: https://www.sciencedirect.com/science/article/pii/S004896971732171X.

Eldeiry, A., 2012. Evaluating the performance of ordinary kriging in mapping soil salinity. J. Irrig. Drain. Eng. 138, 1046–1059. http://dx.doi.org/10.1061/(ASCE)IR.1943-4774.0000517.

Essou, G., Brissette, F., Lucas-Picher, P., 2017. The use of reanalyses and gridded observations as weather input data for a hydrological model: Comparison of performances of simulated river flows based on the density of weather stations. J. Hydrometeorol. 18, 497–513. http://dx.doi.org/10.1175/JHM-D-16-0088.1.

Ficchì, A., Perrin, C., Andréassian, V., 2016. Impact of temporal resolution of inputs on hydrological model performance: An analysis based on 2400 flood events. J. Hydrol. 538, 454–470. http://dx.doi.org/10.1016/j.jhydrol.2016.04.016, URL: https://www.sciencedirect.com/science/article/pii/S0022169416301974.

Frei, C., Schär, C., 1998. A precipitation climatology of the Alps from high-resolution rain-gauge observations. Int. J. Climatol. 18 (8), 873–900. http://dx.doi.org/10.1002/(SICI)1097-0088(19980630)18:8<873::AID-JOC255>3.0.CO;2-9.

Galletti, A., Avesani, D., Bellin, A., Majone, B., 2021. Detailed simulation of storage hydropower systems in large Alpine watersheds. J. Hydrol. 603, 127125. http://dx.doi.org/10.1016/j.jhydrol.2021.127125, URL: https://www.sciencedirect.com/science/article/pii/S0022169421011756.

Gentile, M., Courbin, F., Meylan, G., 2012. Interpolating point spread function anisotropy. Astron. Astrophys. 549, http://dx.doi.org/10.1051/0004-6361/201219739.

Ghimire, G.R., Krajewski, W.F., Ayalew, T.B., Goska, R., 2022. Hydrologic investigations of radar-rainfall error propagation to rainfall-runoff model hydrographs. Adv. Water Resour. 161, 104145. http://dx.doi.org/10.1016/j.advwatres.2022.104145, URL: https://www.sciencedirect.com/science/article/pii/S0309170822000239.

Girons Lopez, M., Vis, M.J.P., Jenicek, M., Griessinger, N., Seibert, J., 2020. Assessing the degree of detail of temperature-based snow routines for runoff modelling in mountainous areas in central Europe. Hydrol. Earth Syst. Sci. 24 (9), 4441–4461. http://dx.doi.org/10.5194/hess-24-4441-2020, URL: https://hess.copernicus.org/articles/24/4441/2020/.

Goovaerts, P., 1997. Geostatistics for Natural Resources Evaluation. In: Applied Geostatistics Series, Oxford University Press.

Hafizi, H., Sorman, A., 2022. Assessment of 13 gridded precipitation datasets for hydrological modeling in a mountainous basin. Atmosphere 13 (1), http://dx.doi.org/10.3390/atmos13010143.

Hamill, T.M., Whitaker, J.S., 2006. Probabilistic quantitative precipitation forecasts based on reforecast analogs: Theory and application. Mon. Weather Rev. 134 (11), 3209–3229. http://dx.doi.org/10.1175/MWR3237.1, URL: https://journals.ametsoc.org/view/journals/mwre/134/11/mwr3237.1.xml. Publisher: American Meteorological Society Section: Monthly Weather Review.

Hargreaves, G., Samani, Z., 1985. Reference crop evapotranspiration from temperature. Appl. Eng. Agric. 1, http://dx.doi.org/10.13031/2013.26773.

Hassler, B., Lauer, A., 2021. Comparison of reanalysis and observational precipitation datasets including ERA5 and WFDE5. Atmosphere 12 (11), http://dx.doi.org/10.3390/atmos12111462, URL: https://www.mdpi.com/2073-4433/12/11/1462.

Hersbach, H., Bell, B., Berrisford, P., Biavati, G., Horànyi, A., Muñoz Sabater, J., Nicolas, J., Peubey, C., Radu, R., Rozum, I., Schepers, D., Simmons, A., Soci, C., Dee, D., Thèpaut, J.-N., 2023. ERA5 Hourly Data on Single Levels from 1940 to Present. Copernicus Climate Change Service (C3S) Climate Data Store (CDS), http://dx.doi.org/10.24381/cds.adbb2d47, (Accessed on 01-Jul-2022).

Hersbach, H., Bell, B., Berrisford, P., Hirahara, S., Horányi, A., Muñoz-Sabater, J., Nicolas, J., Peubey, C., Radu, R., Schepers, D., Simmons, A., Soci, C., Abdalla, S., Abellan, X., Balsamo, G., Bechtold, P., Biavati, G., Bidlot, J., Bonavita, M., De Chiara, G., Dahlgren, P., Dee, D., Diamantakis, M., Dragani, R., Flemming, J., Forbes, R., Fuentes, M., Geer, A., Haimberger, L., Healy, S., Hogan, R.J., Hólm, E., Janisková, M., Keeley, S., Laloyaux, P., Lopez, P., Lupu, C., Radnoti, G., de Rosnay, P., Rozum, I., Vamborg, F., Villaume, S., Thépaut, J.-N., 2020. The ERA5 global reanalysis. Q. J. R. Meteorol. Soc. 146 (730), 1999–2049. http://dx.doi.org/10.1002/qj.3803.

Hofstra, N., New, M., McSweeney, C., 2010. The influence of interpolation and station network density on the distributions and trends of climate variables in gridded daily data. Clim. Dynam. 35 (5), 841–858. http://dx.doi.org/10.1007/s00382-009-0698-1, Zie http://www.springerlink.com/content/y392m3k888350478/.

Huang, X., Han, S., Shi, C., 2022. Evaluation of three air temperature reanalysis datasets in the alpine region of the Qinghai–Tibet plateau. Remote Sens. 14 (18), 4447. http://dx.doi.org/10.3390/rs14184447.

Hunziker, S., Gubler, S., Calle, J., Moreno, I., Andrade, M., Velarde, F., Ticona, L., Carrasco, G., Castellón, Y., Oria, C., Croci-Maspoli, M., Konzelmann, T., Rohrer, M., Brönnimann, S., 2017. Identifying, attributing, and overcoming common data quality issues of manned station observations. Int. J. Climatol. 37 (11), 4131–4145. http://dx.doi.org/10.1002/joc.5037.

Isotta, F., Frei, C., 2013. APGD: Alpine precipitation grid dataset. http://dx.doi.org/10.18751/CLIMATE/GRIDDATA/APGD/1.0, URL: http://www.meteoswiss.admin.ch/home/services-and-publications/produkte.subpage.html/en/data/products/2015/alpine-precipitation.html. Medium: NetCDF Type: dataset.

Isotta, F.A., Vogel, P., Frei, C., 2015. Evaluation of European regional reanalyses and downscalings for precipitation in the Alpine region. Meteorol. Z. 24 (1), 15–37. http://dx.doi.org/10.1127/metz/2014/0584.

Khan, S., Shukla, S., Arismendi, I., Grant, G., Lewis, S., Nolin, A., 2016. Influence of winter season climate variability on snow–precipitation ratio in the Western United States. Int. J. Climatol. 36, 3175–3190. http://dx.doi.org/10.1002/joc.4545.

Kouadio, C.A., Kouassi, K.L., Diedhiou, A., Obahoundje, S., Amoussou, E., Kamagate, B., Paturel, J.-e., Coulibaly, T.J.H., Coulibaly, H.S.J.P., Didi, R.S., Savane, I., 2022. Assessing the hydropower potential using hydrological models and geospatial tools in the White Bandama watershed (Côte d'Ivoire, West Africa). Front. Water 4, http://dx.doi.org/10.3389/frwa.2022.844934, URL: https://www.frontiersin.org/article/10.3389/frwa.2022.844934.

Laiti, L., Mallucci, S., Piccolroaz, S., Bellin, A., Zardi, D., Fiori, A., Nikulin, G., Majone, B., 2018. Testing the hydrological coherence of high–resolution gridded precipitation and temperature data sets. Water Resour. Res. 54 (3), 1999–2016. http://dx.doi.org/10.1002/2017WR021633, URL: https://onlinelibrary.wiley.com/doi/abs/10.1002/2017WR021633. Number: 3.

Landelius, T., Dahlgren, P., Gollvik, S., Jansson, A., Olsson, E., 2016. A high-resolution regional reanalysis for Europe. Part 2: 2D analysis of surface temperature, precipitation and wind. Q. J. R. Meteorol. Soc. 142 (698), 2132–2142. http://dx.doi.org/10.1002/qj.2813.

Larsen, S., Majone, B., Zulian, P., Stella, E., Bellin, A., Bruno, M.C., Zolezzi, G., 2021. Combining hydrologic simulations and stream-network models to reveal flow-ecology relationships in a large Alpine catchment. Water Resour. Res. 57 (4), e2020WR028496. http://dx.doi.org/10.1029/2020WR028496, e2020WR028496 2020WR028496.

Lehmann, E.L., Romano, J.P., 1986. Testing Statistical Hypotheses, vol. 3, Springer, New York.

Lespinas, F., Fortin, V., Roy, G., Rasmussen, P., Stadnyk, T., 2015. Performance evaluation of the Canadian precipitation analysis (CaPA). J. Hydrometeorol. 16, 150805113252003. http://dx.doi.org/10.1175/JHM-D-14-0191.1.

Lutz, S.R., Mallucci, S., Diamantini, E., Majone, B., Bellin, A., Merz, R., 2016. Hydroclimatic and water quality trends across three Mediterranean river basins. Sci. Total Environ. 571, 1392–1406. http://dx.doi.org/10.1016/j.scitotenv.2016.07.102.

Ly, S., Charles, C., Degré, A., 2013. Different methods for spatial interpolation of rainfall data for operational hydrology and hydrological modeling at watershed scale: a review. Biotechnol. Agron. Soc. Environ. 17 (2), URL: https://orbi.uliege.be/handle/2268/136084. Publisher: Presses Agronomiques de Gembloux, Gembloux, Belgium.

Madhavi, G., Sharath Kumar, P., Chipade, R., Bhate, J., Sarma, T., 2022. Estimation and validation study of soil moisture using GPS-IR technique over a tropical region: Variability of SM with rainfall and energy fluxes. IEEE J. Sel. Top. Appl. Earth Obs. Remote Sens. 15, 42–49. http://dx.doi.org/10.1109/JSTARS.2021.3127469.

Mahmud, M.A.P., Huda, N., Farjana, S.H., Lang, C., 2019. A strategic impact assessment of hydropower plants in alpine and non-alpine areas of Europe. Appl. Energy 250, 198–214. http://dx.doi.org/10.1016/j.apenergy.2019.05.007, URL: https://www.sciencedirect.com/science/article/pii/S030626191930861X.

Maina, F.Z., Siirila-Woodburn, E.R., Vahmani, P., 2020. Sensitivity of meteorological-forcing resolution on hydrologic variables. Hydrol. Earth Syst. Sci. 24 (7), 3451–3474. http://dx.doi.org/10.5194/hess-24-3451-2020, URL: https://hess.copernicus.org/articles/24/3451/2020/.

Majone, B., Villa, F., Deidda, R., Bellin, A., 2016. Impact of climate change and water use policies on hydropower potential in the south-eastern Alpine region. Sci. Total Environ. 543, 965–980. http://dx.doi.org/10.1016/j.scitotenv.2015.05.009, URL: https://www.sciencedirect.com/science/article/pii/S004896971530067X.

Mallucci, S., Majone, B., Bellin, A., 2019. Detection and attribution of hydrological changes in a large Alpine river basin. J. Hydrol. 575, 1214–1229. http://dx.doi.org/10.1016/j.jhydrol.2019.06.020, URL: https://www.sciencedirect.com/science/article/pii/S0022169419305712.

Mastrantonas, N., Furnari, L., Magnusson, L., Senatore, A., Mendicino, G., Pappenberger, F., Matschullat, J., 2022. Forecasting extreme precipitation in the central Mediterranean: Changes in predictors' strength with prediction lead time. Meteorol. Appl. 29 (6), e2101. http://dx.doi.org/10.1002/met.2101, URL: https://rmets.onlinelibrary.wiley.com/doi/abs/10.1002/met.2101. arXiv:https://rmets.onlinelibrary.wiley.com/doi/pdf/10.1002/met.2101.

Melsen, L., Teuling, A., Torfs, P., Zappa, M., Mizukami, N., Clark, M., Uijlenhoet, R., 2016. Representation of spatial and temporal variability in large-domain hydrological models: Case study for a mesoscale pre-Alpine basin. Hydrol. Earth Syst. Sci. 20, 2207–2226. http://dx.doi.org/10.5194/hess-20-2207-2016.

Menne, M., Williams, C., Gleason, B., Rennie, J., Lawrimore, J., 2018. The global historical climatology network monthly temperature dataset, version 4. J. Clim. 31, http://dx.doi.org/10.1175/JCLI-D-18-0094.1.

Michelon, A., Benoit, L., Beria, H., Ceperley, N., Schaefli, B., 2021. Benefits from high-density rain gauge observations for hydrological response analysis in a small alpine catchment. Hydrol. Earth Syst. Sci. 25 (4), 2301–2325. http://dx.doi.org/10.5194/hess-25-2301-2021, URL: https://hess.copernicus.org/articles/25/2301/2021/. Publisher: Copernicus GmbH.

Mistry, M.N., Schneider, R., Masselot, P., Royé, D., Armstrong, B., Kyselý, J., Orru, H., Sera, F., Tong, S., Lavigne, E., Urban, A., Madureira, J., García-León, D., Ibarreta, D., Ciscar, J.-C., Feyen, L., de Schrijver, E., de Sousa Zanotti Stagliorio Coelho, M., Pascal, M., Tobias, A., Guo, Y., Vicedo-Cabrera, A.M., Gasparrini, A., 2022. Comparison of weather station and climate reanalysis data for modelling temperature-related mortality. Sci. Rep. 12 (1), 5178. http://dx.doi.org/10.1038/s41598-022-09049-4.

Monteiro, D., Caillaud, C., Samacoïts, R., Lafaysse, M., Morin, S., 2022. Potential and limitations of convection-permitting CNRM-AROME climate modelling in the French Alps. Int. J. Climatol. 42 (14), 7162–7185. http://dx.doi.org/10.1002/joc.7637.

Monteiro, D., Morin, S., 2023. Multi-decadal past winter temperature, precipitation and snow cover information over the European Alps using multiple datasets. EGUsphere 2023, 1–62. http://dx.doi.org/10.5194/egusphere-2023-166, URL: https://egusphere.copernicus.org/preprints/2023/egusphere-2023-166/.

Moore, R.J., 2007. The PDM rainfall-runoff model. Hydrol. Earth Syst. Sci. 11 (1), 483–499. http://dx.doi.org/10.5194/hess-11-483-2007, URL: https://hess.copernicus.org/articles/11/483/2007/. Publisher: Copernicus GmbH.

Moriasi, D.N., Arnold, J.G., Liew, M., Bingner, R.L., Harmel, R.D., Veith, T.L., 2007. Model evaluation guidelines for systematic quantification of accuracy in watershed simulations. Trans. ASABE 50, 885–900.

Muñoz Sabater, J., Dutra, E., Agustí-Panareda, A., Albergel, C., Arduini, G., Balsamo, G., Boussetta, S., Choulga, M., Harrigan, S., Hersbach, H., Martens, B., Miralles, D.G., Piles, M., Rodríguez-Fernández, N.J., Zsoter, E., Buontempo, C., Thépaut, J.N., 2021. Era5-land: A state-of-the-art global reanalysis dataset for land applications. Earth Syst. Sci. Data Discuss. 1–50. http://dx.doi.org/10.5194/essd-2021-82, URL: https://essd.copernicus.org/preprints/essd-2021-82/. publisher: Copernicus GmbH.

Murphy, K.P., 2012. Machine Learning: A Probabilistic Perspective. MIT Press.

Nash, J.E., Sutcliffe, J.V., 1970. River flow forecasting through conceptual models part I — A discussion of principles. J. Hydrol. 10 (3), 282–290. http://dx.doi.org/10.1016/0022-1694(70)90255-6, URL: https://www.sciencedirect.com/science/article/pii/0022169470902556.

National Center for Atmospheric Research, 2016. The climate data guide: Atmospheric reanalysis: Overview & comparison tables. https://climatedataguide.ucar.edu/climate-data/atmospheric-reanalysis-overview-comparison-tables. Online; accessed 02 January 2022.

Nicòtina, L., Alessi Celegon, E., Rinaldo, A., Marani, M., 2008. On the impact of rainfall patterns on the hydrologic response. Water Resour. Res. 44 (12), http://dx.doi.org/10.1029/2007WR006654.

Nijssen, B., Lettenmaier, D.P., 2004. Effect of precipitation sampling error on simulated hydrological fluxes and states: Anticipating the Global Precipitation Measurement satellites. J. Geophys. Res.: Atmos. 109 (D2), http://dx.doi.org/10.1029/2003JD003497.

Norbiato, D., Borga, M., Degli Esposti, S., Gaume, E., Anquetin, S., 2008. Flash flood warning based on rainfall thresholds and soil moisture conditions: An assessment for gauged and ungauged basins. J. Hydrol. 362 (3), 274–290. http://dx.doi.org/10.1016/j.jhydrol.2008.08.023, URL: https://www.sciencedirect.com/science/article/pii/S0022169408004587.

Norbiato, D., Borga, M., Merz, R., Blöschl, G., Carton, A., 2009. Controls on event runoff coefficients in the eastern Italian Alps. J. Hydrol. 375 (3), 312–325. http://dx.doi.org/10.1016/j.jhydrol.2009.06.044, URL: https://www.sciencedirect.com/science/article/pii/S0022169409003485.

Pandey, A., Lalrempuia, D., Jain, S., 2015. Assessment of hydropower potential using spatial technology and SWAT modelling in the Mat River, southern Mizoram, India. Hydrol. Sci. J. 60 (10), 1651–1665. http://dx.doi.org/10.1080/02626667.2014.943669, arXiv:https://doi.org/10.1080/02626667.2014.943669.

Parker, W., 2016. Reanalyses and observations: What's the difference? Bull. Am. Meteorol. Soc. 97, 160128144638003. http://dx.doi.org/10.1175/BAMS-D-14-00226.1.

Pelosi, A., Terribile, F., D'Urso, G., Chirico, G.B., 2020. Comparison of ERA5-land and UERRA MESCAN-SURFEX reanalysis data with spatially interpolated weather observations for the regional assessment of reference evapotranspiration. Water 12 (6), 1669. http://dx.doi.org/10.3390/w12061669, URL: https://www.mdpi.com/2073-4441/12/6/1669. Number: 6 Publisher: Multidisciplinary Digital Publishing Institute.

Prein, A.F., Gobiet, A., 2017. Impacts of uncertainties in European gridded precipitation observations on regional climate analysis. Int. J. Climatol. 37 (1), 305–327. http://dx.doi.org/10.1002/joc.4706.

Prömmel, K., Geyer, B., Jones, J.M., Widmann, M., 2010. Evaluation of the skill and added value of a reanalysis-driven regional simulation for Alpine temperature. Int. J. Climatol. 30 (5), 760–773. http://dx.doi.org/10.1002/joc.1916.

Qiaohong, S., Miao, C., Duan, Q., Ashouri, H., Sorooshian, S., Hsu, K., 2017. A review of global precipitation data sets: Data sources, estimation, and intercomparisons. Rev. Geophys. 56, http://dx.doi.org/10.1002/2017RG000574.

Raffa, M., Reder, A., Marras, G.F., Mancini, M., Scipione, G., Santini, M., Mercogliano, P., 2021. VHR-REA_IT dataset: Very high resolution dynamical downscaling of ERA5 reanalysis over Italy by COSMO-CLM. Data 6 (8), http://dx.doi.org/10.3390/data6080088.

Reder, A., Raffa, M., Padulano, R., Rianna, G., Mercogliano, P., 2022. Characterizing extreme values of precipitation at very high resolution: An experiment over twenty European cities. Weather Clim. Extrem. 35, 100407. http://dx.doi.org/10.1016/j.wace.2022.100407, URL: https://www.sciencedirect.com/science/article/pii/S2212094722000019.

Ruelland, D., 2020. Should altitudinal gradients of temperature and precipitation inputs be inferred from key parameters in snow-hydrological models? Hydrol. Earth Syst. Sci. 24 (5), 2609–2632. http://dx.doi.org/10.5194/hess-24-2609-2020, URL: https://hal.umontpellier.fr/hal-03202749. Publisher: European Geosciences Union.

Rysman, J.-F., Lemaître, Y., Moreau, E., 2016. Spatial and temporal variability of rainfall in the Alps–Mediterranean Euroregion. J. Appl. Meteorol. Climatol. 55 (3), 655–671. http://dx.doi.org/10.1175/JAMC-D-15-0095.1, Publisher: American Meteorological Society; Section: Journal of Applied Meteorology and Climatology.

Scherrer, S., 2020. Temperature monitoring in mountain regions using reanalyses: Lessons from the Alps. Environ. Res. Lett. 15, 044005. http://dx.doi.org/10.1088/1748-9326/ab702d.

Shrestha, S., Zaramella, M., Callegari, M., Greifeneder, F., Borga, M., 2023. Scale dependence of errors in snow water equivalent simulations using ERA5 reanalysis over alpine basins. Climate 11 (7), 154. http://dx.doi.org/10.3390/cli11070154.

Shuai, P., Chen, X., Mital, U., Coon, E.T., Dwivedi, D., 2022. The effects of spatial and temporal resolution of gridded meteorological forcing on watershed hydrological responses. Hydrol. Earth Syst. Sci. 26 (8), 2245–2276. http://dx.doi.org/10.5194/hess-26-2245-2022, URL: https://hess.copernicus.org/articles/26/2245/2022/.

Sideris, I.V., Gabella, M., Erdin, R., Germann, U., 2014. Real-time radar–rain-gauge merging using spatio-temporal co-kriging with external drift in the alpine terrain of Switzerland. Q. J. R. Meteorol. Soc. 140 (680), 1097–1111. http://dx.doi.org/10.1002/qj.2188.

Simmons, A.J., Berrisford, P., Dee, D.P., Hersbach, H., Hirahara, S., Thépaut, J.-N., 2017. A reassessment of temperature variations and trends from global reanalyses and monthly surface climatological datasets. Q. J. R. Meteorol. Soc. 143 (702), 101–119. http://dx.doi.org/10.1002/qj.2949.

Simmons, A., Uppala, S., Dee, D., Kobayashi, S., 2006. ERA-Interim: New ECMWF reanalysis products from 1989 onwards. ECMWF Newsl. 110, 26–35. http://dx.doi.org/10.21957/pocnex23c6, Thanks to ICDC, CEN, University of Hamburg for data support.

Sood, A., Smakhtin, V., 2015. Global hydrological models: a review. Hydrol. Sci. J. 60 (4), 549–565. http://dx.doi.org/10.1080/02626667.2014.950580, Publisher: Taylor & Francis _eprint: https://doi.org/10.1080/02626667.2014.950580.

Stergiadi, M., Di Marco, N., Avesani, D., Righetti, M., Borga, M., 2020. Impact of geology on seasonal hydrological predictability in alpine regions by a sensitivity analysis framework. Water 12 (8), 2255. http://dx.doi.org/10.3390/w12082255, URL: https://www.mdpi.com/2073-4441/12/8/2255. Number: 8 Publisher: Multidisciplinary Digital Publishing Institute.

Tapiador, F., Navarro, A., Levizzani, V., Garcìa-Ortega, E., Huffman, G., Kidd, C., Kucera, P., Kummerow, C., Masunaga, H., Petersen, W., Roca, R., Sànchez, J.-L., Tao, W.-K., Turk, F., 2017. Global precipitation measurements for validating climate models. Atmos. Res. 197, 1–20. http://dx.doi.org/10.1016/j.atmosres.2017.06.021, URL: https://www.sciencedirect.com/science/article/pii/S0169809517303861.

Tarek, M., Brissette, F.P., Arsenault, R., 2020. Evaluation of the ERA5 reanalysis as a potential reference dataset for hydrological modelling over North America. Hydrol. Earth Syst. Sci. 24 (5), 2527–2544. http://dx.doi.org/10.5194/hess-24-2527-2020, URL: https://hess.copernicus.org/articles/24/2527/2020/. Publisher: Copernicus GmbH.

Tetzner, D., Thomas, E., Allen, C., 2019. A validation of ERA5 reanalysis data in the Southern Antarctic Peninsula—Ellsworth land region, and its implications for ice core studies. Geosciences 9 (7), 289. http://dx.doi.org/10.3390/geosciences9070289, URL: https://www.mdpi.com/2076-3263/9/7/289. Number: 7 Publisher: Multidisciplinary Digital Publishing Institute.

Tian, Y., Huffman, G.J., Adler, R.F., Tang, L., Sapiano, M., Maggioni, V., Wu, H., 2013. Modeling errors in daily precipitation measurements: Additive or multiplicative? Geophys. Res. Lett. 40 (10), 2060–2065. http://dx.doi.org/10.1002/grl.50320.

Tuo, Y., Duan, Z., Disse, M., Chiogna, G., 2016. Evaluation of precipitation input for SWAT modeling in Alpine catchment: A case study in the Adige river basin (Italy). Sci. Total Environ. 573, 66–82. http://dx.doi.org/10.1016/j.scitotenv.2016.08.034, URL: https://www.sciencedirect.com/science/article/pii/S0048969716317260.

Volpi, E., Di Lazzaro, M., Fiori, A., 2012. A simplified framework for assessing the impact of rainfall spatial variability on the hydrologic response. Adv. Water Resour. 46, 1–10. http://dx.doi.org/10.1016/j.advwatres.2012.04.011, URL: https://www.sciencedirect.com/science/article/pii/S0309170812000954.

Weerts, A.H., Winsemius, H.C., Verkade, J.S., 2011. Estimation of predictive hydrological uncertainty using quantile regression: examples from the National Flood Forecasting System (England and Wales). Hydrol. Earth Syst. Sci. 15 (1), 255–265. http://dx.doi.org/10.5194/hess-15-255-2011, URL: https://hess.copernicus.org/articles/15/255/2011/hess-15-255-2011.html. Publisher: Copernicus GmbH.

Wetterhall, F., He, Y., Cloke, H., Pappenberger, F., 2011. Effects of temporal resolution of input precipitation on the performance of hydrological forecasting. Adv. Geosci. 29, 21–25. http://dx.doi.org/10.5194/adgeo-29-21-2011, URL: https://adgeo.copernicus.org/articles/29/21/2011/.

Woelber, B., Maneta, M.P., Harper, J., Jencso, K.G., Gardner, W.P., Wilcox, A.C., López-Moreno, I., 2018. The influence of diurnal snowmelt and transpiration on hillslope throughflow and stream response. Hydrol. Earth Syst. Sci. 22 (8), 4295–4310. http://dx.doi.org/10.5194/hess-22-4295-2018, URL: https://hess.copernicus.org/articles/22/4295/2018/.

Xie, W., Yi, S., Leng, C., Xia, D., Li, M., Zhong, Z., Ye, J., 2022. The evaluation of IMERG and ERA5-Land daily precipitation over China with considering the influence of gauge data bias. Sci. Rep. 12 (1), 8085. http://dx.doi.org/10.1038/s41598-022-12307-0.

Xu, J., Liu, T., 2021. Optimal hourly scheduling for wind-hydropower systems with integrated pumped-storage technology. J. Energy Eng. 147 (3), 04021013. http://dx.doi.org/10.1061/(ASCE)EY.1943-7897.0000728.

Xue, Y., Janjic, Z., Dudhia, J., Vasic, R., De Sales, F., 2014. A review on regional dynamical downscaling in intraseasonal to seasonal simulation/prediction and major factors that affect downscaling ability. Atmos. Res. 147–148, 68–85. http://dx.doi.org/10.1016/j.atmosres.2014.05.001, URL: https://www.sciencedirect.com/science/article/pii/S0169809514002002.

Zandler, H., Senftl, T., Vanselow, K.A., 2020. Reanalysis datasets outperform other gridded climate products in vegetation change analysis in peripheral conservation areas of Central Asia. Sci. Rep. 10 (1), 22446. http://dx.doi.org/10.1038/s41598-020-79480-y.

Zaramella, M., Borga, M., Zoccatelli, D., Carturan, L., 2019. TOPMELT 1.0: a topography-based distribution function approach to snowmelt simulation for hydrological modelling at basin scale. Geosci. Model Dev. 12 (12), 5251–5265. http://dx.doi.org/10.5194/gmd-12-5251-2019, URL: https://gmd.copernicus.org/articles/12/5251/2019/.

Zhang, F., Zhang, H., Hagen, S.C., Ye, M., Wang, D., Gui, D., Zeng, C., Tian, L., Liu, J., 2015. Snow cover and runoff modelling in a high mountain catchment with scarce data: effects of temperature and precipitation parameters. Hydrol. Process. 29 (1), 52–65. http://dx.doi.org/10.1002/hyp.10125.